Supporting Information

Pursuing the Complete OFF State in Photoswitchable Catalysis

Mykola Kravets,[a] Matteo Flaibani,[b] Magdalena Szewczyk,[a] Paola Posocco,*[b] and Volodymyr Sashuk*[a]

[a] *Institute of Physical Chemistry, Polish Academy of Sciences, Kasprzaka 44/52, 01-224 Warsaw, Poland*

[b] *Department of Engineering and Architecture, University of Trieste,* 34127 Trieste, Italy

E-mail: paola.posocco@dia.units.it, vsashuk@ichf.edu.pl

Table of Contents

1. General Information

1.1 Experimental conditions

All chemicals were purchased as reagent grade from commercial suppliers (Merck, Alfa Aesar, TCI) and used without further purification. The solvents used (Merck, ChemPur, PoCh) were of analytical grade quality. Deuterated solvents were purchased from Armar Chemicals. Methylene chloride (DCM) and acetonitrile (ACN) were dried over CaH2 and distilled under argon atmosphere. Acetone was dried over 4A Linde molecular sieves and then distilled under argon atmosphere. Methanol (MeOH) was dried over 3A molecular sieves and then distilled under argon atmosphere**.** Deionized water (18.3 MΩ·cm) was obtained from Milli-Q station. Experiments were performed at room temperature unless otherwise noted. The progress of organic reactions was monitored by thin layer chromatography (TLC) using Merck silica gel 60 F254 (0.2 mm) on alumina plates. The products were purified by column chromatography (CC) using Merck silica gel 60 (230-400 mesh ASTM). NMR spectra were recorded on Bruker 400 MHz instrument, and analyzed using MestReNova software. The chemical shifts (δ) are given in ppm relative to TMS, coupling constants are (*J*) in Hz. Quartz cuvettes were purchased from Hellma Analytics. Absorbance spectra were recorded using Evolution220 spectrophotometer from Thermo Scientific, and analyzed using Origin software. Photoswitching was accomplished using RF-6000 spectrofluorometer from Shimadzu. High-resolution ESI mass spectra were recorded on SYNAPT spectrometer. X-ray photoelectron spectra (XPS) were recorded on a PHI 5000 VersaProbe (ULVAC-PHI) spectrometer, and analyzed using CasaXPS software. TEM images were recorded on FEI TECNAI and analyzed by ImageJ program. Thermogravimetric analysis (TGA) was performed using Mettler Toledo TGA/DSC 3+ instrument.

1.2 Computational methods

Atomistic models
The gold (Au) core of the nanoparticle model considered here is an icosahedron of ~3.0 nm in size, built using the Atomistic Simulation Environment (ASE)[1], a lattice constant of ~0.41 nm and a material density of 19.3 g/cm^3. Each nanoparticle is decorated with 155 ligands uniformly arranged on the Au surface. Interactions between Au atoms were described using the parameters of INTERFACE[2] force field for metals. The PT, SAT, and HDT ligands were parametrized according to the gaff2[3] force field. The RED server was employed to derive the atomic partial charges, applying the RESP fitting method.[4-8] To account for the photoinduced isomerization of the azobenzene we adopted the modified dihedral potential proposed by Heinz et al.[9-11], which is able to produce a spontaneous *trans→cis* and *cis→trans* isomerization of the azobenzene within picoseconds of molecular dynamics (MD) simulations, by temporarily changing the central CNNC dihedral potential term of the azo group.
Due the presence of the complex Ru metal center, a fragment based approach was adopted for the derivation of gaff2-compatible bond parameters and atomic charges for the SAT(Ru) ligand; accordingly, the ligand was divided into two parts, the first one containing the Hoveyda-Grubbs catalytic center and the second one the remaining atoms; the blocks were parametrized separately first and then merged together. In particular, the Hoveyda-Grubbs group molecular model was built starting from literature[12] and then the geometry was optimized in gas phase at the DFT level of theory using the B3LYP[13] hybrid functional, a 6-31G(d,p)[14,15] basis set for the main group elements, and the quasi relativistic effective core pseudo-potentials (RECP) of the Stuttgart group[16,17] for Ru.[12,18] DFT calculations were carried out within the ORCA[19] program.

The atomistic force field parameters for the metal-containing group were derived using the Seminario's method following the VFFDT protocol.[20] Partial atomic charges were calculated as explained above on the energy-minimized molecular structure.

The *tleap* program implemented in AMBER 20[21] suite of programs was used to solvate the functionalized nanoparticle with a cubic box of dichloromethane molecules, placing at least 18 Å of solvent from each solute atom.

Molecular dynamics simulations

The MD simulations were performed using the GPU (CUDA) version of PMEMD engine[22-24] implemented in AMBER 20. The position of the Au atoms and the sulfurs of the thiol groups were restrained during the simulation steps. The solvent was first minimized while keeping the other atoms fixed, to avoid bad contacts between the solvent molecules and the solute, then the whole system was subjected to minimization. Both the steps used a combination of steepest descent and conjugate gradient, and a cutoff of 10 Å for the nonbonded interactions. Temperature was then slowly brought to 300 K (integration step of 1 fs) in the canonical NVT ensemble. Later, the system was equilibrated (integration step of 2 fs) at constant temperature (300 K) and pressure (1 atm) using the Berendsen barostat for 10 ns and the Monte Carlo barostat for the following 10 ns. Production phase was then carried out in NPT canonical ensemble (T=300 K, Monte Carlo barostat) for further 100 ns. In all the simulations, the SHAKE algorithm was used to restrain the bonds involving hydrogen atoms. Periodic boundary conditions (PBC) were employed, and the electrostatic interactions were computed with the Particle Mesh Ewald (PME) algorithm, with a cutoff of 10 Å.

1D Umbrella sampling

The C-N-N-C dihedral of the azobenzene linker was chosen as a single collective variable to investigate the conversion from the *cis* to the *trans* isomer by means of Umbrella Sampling (US) calculations. A total of 64 windows was simulated, spanning from 0.00 to 3.14 radians, and spaced by ~0.05 radians. A constant of 100 kcal/mol·rad^2 was used to define the harmonic potential. For the unbound ligands (free in solvent, used as a reference) each window was simulated for a total of 150 ps, discarding the first 50 ps as equilibration, while for the ligands grafted to the NP the total time was of 1.2 ns, and the first 200 ps were not considered. The same settings used for the MD simulations were used also here. The windows were simulated in series, using the last frame of the previous window as starting point. The free energy curve was then reconstructed using the Weighted Histogram Analysis Method (WHAM)[25-28].

2D Umbrella sampling

The dihedral C-N-N-C and the angle N-N-C of the azobenzene group were chosen as the two collective variables along which study the conversion from the *cis* to the *trans* isomer at a more in-depth level. The angle was first sampled through US simulations in series to obtain starting configurations at different angles. The N-N-C angle was sampled using a constant of 1000 kcal/mol·rad^2, from 1.74 to 2.94 radians, with a spacing of 0.10 radians (13 windows). The dihedral was then sampled in series while keeping fixed the angle, running in parallel the US simulations at different angle values. A constant of 100 kcal/mol·rad^2 was used, sampling from 0.00 to 3.14 with a spacing of ~0.15 radians (22 windows). A total of 286 windows for each system was sampled, each window being simulated for 1.5 ns, with the first 500 ps discarded as equilibration. The Free Energy Surface (FES) was then reconstructed using WHAM.

2. Synthesis of ligands

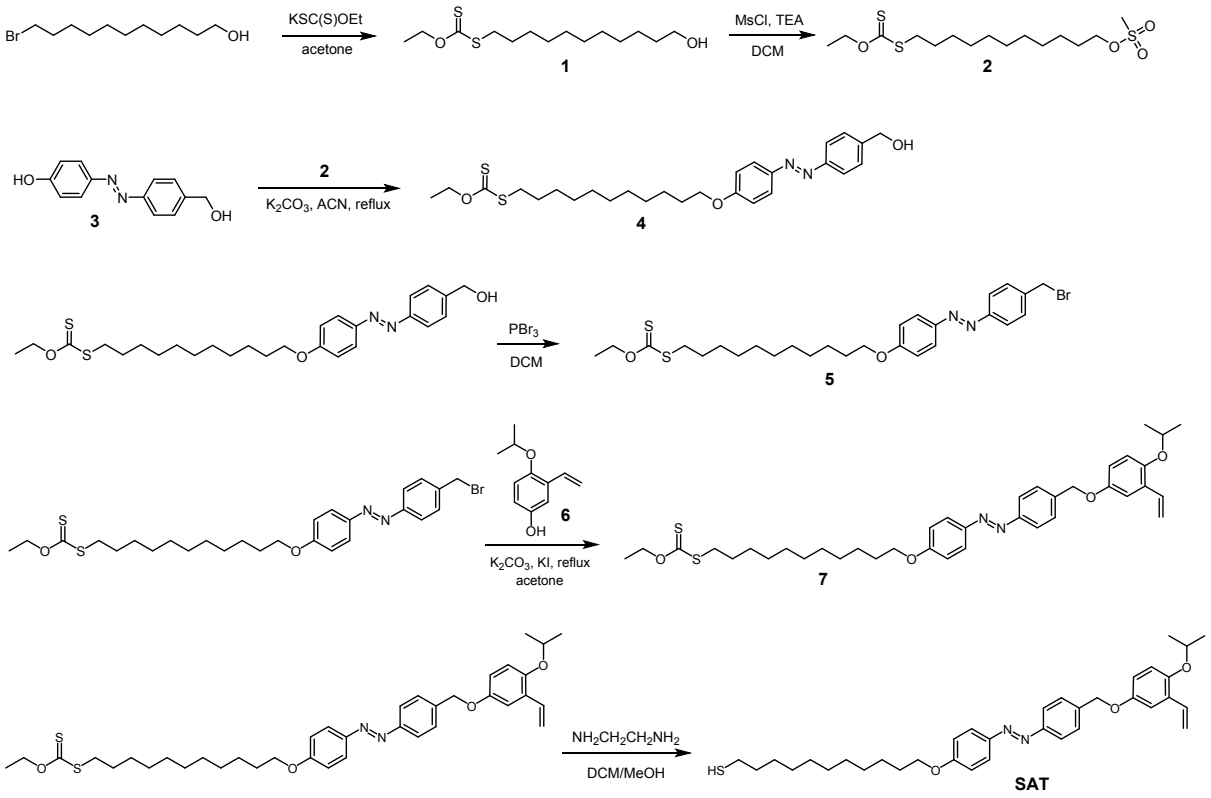

Figure S1**.** Synthetic route to SAT ligand.

O-ethyl S-(11-hydroxyundecyl) carbonodithioate (1): To a stirred solution of 11-bromo-1-undecanol (5 g, 20 mmol) was added potassium ethyl xanthate (3.83 g, 24 mmol) in acetone (60 mL) at room temperature. The reaction mixture was stirred for 24h. The insoluble material was filtered off and the filtrate was concentrated under vacuum. Purification by flash column chromatography on silica (hexane/EtOAc = 4/1) gave **1** (5.6 g, 96%) as a colorless oil. ^{1}H NMR (400 MHz, $CDCl_3$): δ 4.64 (q, *J* = 7.1 Hz, 2H), 3.64 (t, *J* = 6.6 Hz, 2H), 3.15 – 3.07 (m, 2H), 1.67 (tt, *J* = 7.5, 6.6 Hz, 2H), 1.62 – 1.50 (m, 2H), 1.44 (bs, 1H), 1.42 (t, *J* = 7.1 Hz, 3H), 1.44-1.28 (m, 14H). The NMR data agree with those published in the literature.[29]

11-((ethoxycarbonothioyl)thio)undecyl methanesulfonate (2): 1 (5.6g, 19.1 mmol) and 180 mL of dry DCM were added to a 250 mL round bottomed flask under argon atmosphere. The mixture was cooled down to 0 ^{0}C. Then, triethylamine (4 mL, 28.7 mmol) was added followed by dropwise addition of MsCl (1.78 mL, 23.0 mmol). The reaction mixture was allowed to warm up to room temperature and was stirred for 2 h. The solution was washed with 500 mL of brine, dried with anhydrous $MgSO_4$ and concentrated under vacuum to give **2** (7.1 g, 97%) as a colorless oil. ^{1}H NMR (400 MHz, $CDCl_3$): δ 4.64 (q, *J* = 7.1 Hz, 2H), 4.21 (t, *J* = 6.6 Hz, 2H), 3.14 – 3.07 (m, 2H), 2.99 (s, 3H), 1.81 – 1.61 (m, *J* =6.6, 4H), 1.36-1.27 (m, 14H). ^{13}C NMR (100 MHz, $CDCl_3$): δ 215.4, 70.3, 69.9, 37.5, 36.0, 29.5, 29.5, 29.5, 29.2, 29.2, 29.1, 29.0, 28.5, 25.5, 13.9. HRMS (ESI) m/z: calc. for $C_{15}H_{30}O_4S_2Na$: 393.1204 $[M+Na]^+$; found: 393.1208.

(E)-4-((4-(hydroxymethyl)phenyl)diazenyl)phenol (3): Compound **3** was synthesized according to the literature procedure.[30]

(E)-O-ethyl S-(11-(4-((4-(hydroxymethyl)phenyl)diazenyl)phenoxy)undecyl) carbonodithioate (4): A solution of **3** (1.5 g, 6.6 mmol) in dry ACN (180 ml) was treated with **2** (2.83 g, 7.36 mmol) and K_2CO_3 (1.36 g, 9.86 mmol) and a small amount of KI under argon atmosphere. Then, the reaction mixture was refluxed overnight. K_2CO_3 was filtered off and the filtrate was concentrated under vacuum. The crude product was purified by flash column chromatography on silica (hexane/EtOAc = 7/3) to give **4** as an orange solid (2.1 g, 64%). ^{1}H NMR (400 MHz, $CDCl_3$): δ 7.95 – 7.85 (m, 4H), 7.52 – 7.46 (m, 2H), 7.03 – 6.97 (m, 2H), 4.77 (s, 2H), 4.64 (q, *J* = 7.1 Hz, 2H), 4.04 (t, *J* = 6.6 Hz, 2H), 3.15 – 3.07 (m, 3H), 1.87 (bs, 1H), 1.82 (dd, *J* = 8.2, 6.5 Hz, 2H), 1.72 – 1.64 (m, 2H), 1.50 – 1.25 (m, 16H). ^{13}C NMR (100 MHz, $CDCl_3$): δ 215.5, 162.0, 152.3, 146.9, 143.3, 127.6, 125.0, 122.9, 114.9, 69.9, 68.5, 65.1, 36.1, 29.7, 29.6, 29.6, 29.5, 29.3, 29.2, 29.0, 28.5, 26.1, 14.0. HRMS (ESI) m/z: calc. for $C_{27}H_{39}O_3S_2N_2$: 503.2402 $[M+H]^+$; found: 503.2398.

(E)-S-(11-(4-((4-(bromomethyl)phenyl)diazenyl)phenoxy)undecyl) O-ethyl carbonodithioate (5): To a solution of **4** (1 g, 2 mmol) in dry DCM (100 mL) was added PBr_3 (190 µL, 2 mmol) under argon atmosphere at 0 ^{0}C. The resulting mixture was stirred at room temperature overnight. The solution was concentrated under reduce pressure. The residue was purified by column chromatography (hexane/EtOAc = 9/1) to give **5** as an orange solid (860 mg, 77%). ^{1}H NMR (400 MHz, $CDCl_3$): δ 7.95 – 7.88 (m, 2H), 7.92 – 7.81 (m, 2H), 7.58 – 7.48 (m, 2H), 7.04 – 6.88 (m, 2H), 4.63 (dq, *J* = 14.0, 7.1 Hz, 2H), 4.55 (s, 2H), 4.04 (t, *J* = 6.6 Hz, 2H), 3.11 (td, *J* = 7.6, 1.7 Hz, 2H), 1.81 (q, *J* = 6.9 Hz, 2H), 1.77 – 1.64 (m, 2H), 1.53 – 1.30 (m, 17H). ^{13}C NMR (100 MHz, $CDCl_3$): δ 215.5, 162.1, 152.6, 146.9, 139.9, 130.0, 125.1, 123.1, 114.9, 69.9, 68.6, 36.1, 33.1, 29.7, 29.6, 29.6, 29.5, 29.3, 29.3, 29.0, 28.5, 26.2, 14.0. HRMS (ESI) m/z: calc. for $C_{27}H_{38}O_3S_2N_2Br$: 565.1558 $[M+H]^+$; found: 565.1561.

4-isopropoxy-3-vinylphenol (6): Compound **6** was synthesised according to the literature procedure.[31]

(E)-O-ethyl S-(11-(4-((4-((4-isopropoxy-3-vinylphenoxy)methyl)phenyl)-diazenyl)phenoxy)undecyl) carbonodithioate (7): To a stirred solution of **5** (38 mg, 0.068 mmol) and **6** (11 mg, 0.062 mmol) in dry acetone was added K_2CO_3 (17 mg, 0.124 mmol) and KI (11 mg, 0.068 mmol) and refluxed for 48 h. The solution was concentrated under reduced pressure. The residue was purified by column chromatography (hexane/EtOAc = 95/5) to give **7** as an yellow solid (15 mg, 37%). ^{1}H NMR (400 MHz, $CDCl_3$): δ 7.95 – 7.85 (m, 4H), 7.59 – 7.46 (m, 2H), 7.14 (t, *J* = 1.7 Hz, 1H), 7.10 – 6.96 (m, 3H), 6.86 – 6.79 (m, 2H), 5.70 (dd, *J* = 17.8, 1.4 Hz, 1H), 5.24 (dd, *J* = 11.1, 1.4 Hz, 1H), 5.11 (s, 2H), 4.65 (q, *J* = 7.1 Hz, 2H), 4.39 (hept, *J* = 5.8 Hz, 1H), 4.05 (t, *J* = 6.6 Hz, 2H), 3.16 – 3.08 (m, 2H), 1.82 (p, *J* = 6.6 Hz, 2H), 1.75 – 1.65 (m, 2H), 1.42 (t, *J* = 7.1 Hz, 3H), 1.52 – 1.31 (m, 20H). ^{13}C NMR (100 MHz, $CDCl_3$): δ 215.4, 161.9, 153.1, 152.6, 149.9, 147.0, 139.7, 131.9, 129.5, 128.1, 124.9, 122.9, 116.9, 115.3, 114.8, 114.4, 112.7, 72.4, 70.4, 69.9, 68.5, 36.1, 29.7, 29.6, 29.6, 29.5, 29.3, 29.2, 29.0, 28.5, 26.1, 22.4, 14.0. HRMS (ESI) m/z: calc. for $C_{38}H_{51}O_4S_2N_2$: 663.3290 $[M+H]^+$; found: 663.3289.

(E)-11-(4-((4-((4-isopropoxy-3-vinylphenoxy)methyl)phenyl)diazenyl)-phenoxy)undecane-1-thiol (SAT): To a solution of **7** (15 mg, 0.023 mmol) in dry MeOH/DCM (2 mL, v/v 1:1) was added ethylenediamine (9 µL, 0.136 mmol) under argon atmosphere. The temperature was raised to 40 ^{0}C and kept overnight. The solution was concentrated under vacuum. The crude product was purified by flash column chromatography on silica (hexane/EtOAc = 95/5) to give the product as a yellow solid (6.2 mg, 48%). ^{1}H NMR (400 MHz, $CDCl_3$): δ 7.91 (t, *J* = 8.5 Hz, 4H), 7.56 (d, *J* = 8.2 Hz, 2H), 7.14 (t, *J* = 1.8 Hz, 1H), 7.10 – 6.96 (m, 3H), 6.86 – 6.79 (m, 2H), 5.70 (dd, *J* = 17.7, 1.4 Hz, 1H), 5.25 (dd, *J* = 11.1, 1.4 Hz, 1H), 5.11 (s, 2H), 4.39 (hept, *J* = 6.0 Hz, 1H), 4.04 (t, *J* = 6.5 Hz, 2H), 2.53 (q, *J* = 7.4 Hz, 2H), 1.88 – 1.74 (m,

2H), 1.71 (bs, 1H), 1.61 (p, *J* = 7.2 Hz, 2H), 1.54 – 1.20 (m, 20H). ^{13}C NMR (100 MHz, $CDCl_3$): δ 162.0, 153.1, 152.5, 149.9, 147.0, 139.7, 131.9, 129.5, 128.1, 125.0, 122.9, 117.0, 115.3, 114.9, 114.4, 112.7, 72.4, 70.4, 68.5, 34.2, 29.9, 29.7, 29.6, 29.5, 29.3, 29.2, 28.5, 26.2, 24.8, 22.4. HRMS (ESI) m/z: calc. for $C_{35}H_{47}N_2O_3S$: 575.3307 $[M+H]^+$; found: 575.3309.

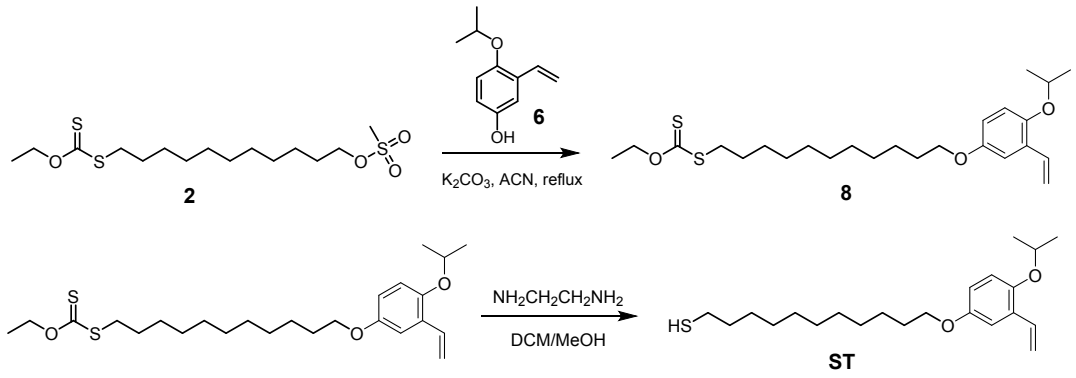

Figure S2**.** Synthetic route to ST ligand.

O-ethyl S-(11-(4-isopropoxy-3-vinylphenoxy)undecyl)carbonodithionate (8): A solution of **6** (200 mg, 1.10 mmol) in dry ACN (25 ml) was treated with **2** (470 mg, 1.26 mmol), K_2CO_3 (230 mg, 1.67 mmol) under argon atmosphere. Then, the reaction mixture was refluxed overnight. K_2CO_3 was filtered off and the filtrate was concentrated under vacuum. The crude product was purified by flash column chromatography on silica (hexane/EtOAc = 95/5) to give **8** as a yellow oil (430 mg, 84%). ^{1}H NMR (400 MHz, $CDCl_3$): δ 7.09 – 6.96 (m, 2H), 6.82 (d, *J* = 8.9 Hz, 1H), 6.75 (dd, *J* = 8.9, 3.0 Hz, 1H), 5.75 – 5.65 (dd, *J* = 17.7, 1.4 Hz, 1H), 5.23 (dd, *J* = 11.1, 1.4 Hz, 1H), 4.64 (m, *J* = 7.1 Hz, 2H), 4.37 (hept, *J* = 6.0 Hz, 1H), 3.92 (t, *J* = 6.6 Hz, 2H), 3.15 – 3.07 (m, 2H), 1.82 – 1.62 (m, 4H), 1.50 – 1.29 (m, 23H). ^{13}C NMR (100 MHz, $CDCl_3$): δ 215.28, 153.49, 149.33, 131.88, 129.29, 117.06, 114.76, 114.03, 111.91, 72.34, 69.73, 68.49, 35.92, 32.19, 29.53, 29.47, 29.43, 29.41, 29.39, 29.10, 28.87, 28.35, 26.06, 22.24, 13.80. HRMS (ESI) m/z: calc. for $C_{25}H_{40}O_3S_2Na$: 475.2317 $[M+Na]^+$; found: 475.2318.

11-(4-isopropoxy-3-vinylphenoxy)undecane-1-thiol (ST): To a solution of **8** (63.5 mg, 0.14 mmol) in dry MeOH/DCM (1:1, 16 mL) was added ethylenediamine (112.4 µL, 1.68 mmol) under argon atmosphere. The temperature was raised to 40^{0}C and kept overnight. The solution was concentrated under vacuum. The crude product was purified by flash column chromatography on silica (hexane/DCM =3/1) to give **ST** as a colorless oil (15 mg, 30%). ^{1}H NMR (400 MHz, $CDCl_3$): δ 7.14 – 6.97 (m, 2H), 6.82 (d, *J* = 8.9 Hz, 1H), 6.75 (dd, *J* = 8.9, 3.0 Hz, 1H), 5.70 (dd, *J* = 17.8, 1.5 Hz, 1H), 5.23 (dd, *J* = 11.1, 1.4 Hz, 1H), 4.37 (p, *J* = 6.1 Hz, 1H), 3.92 (t, *J* = 6.6 Hz, 2H), 2.52 (q, *J* = 7.5 Hz, 2H), 1.76 (tt, *J* = 6.7 Hz, 2H), 1.63 (tt, *J* = 14.8, 7.3 Hz, 2H), 1.45 – 1.23 (m, 21H). ^{13}C NMR (100 MHz, $CDCl_3$): δ 153.49, 149.33, 131.88, 129.30, 117.06, 114.76, 114.03, 111.91, 77.20, 72.35, 68.50, 31.50, 30.12, 29.69, 29.53, 29.49, 29.40, 29.38, 29.05, 28.37, 26.06, 24.65, 22.23. HRMS (ESI) m/z: calc. for $C_{22}H_{37}O_2S$: 365.2514 $[M+H]^+$; found: 365.2516.

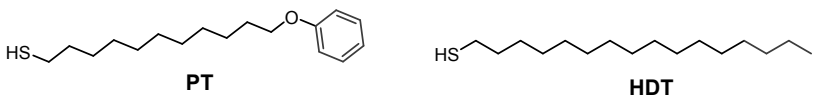

11-phenoxyundecane-1-thiol (PT) and hexadecane-1-thiol (HDT): Ligands **9** and **10** were synthesized according to the literature procedure.[32]

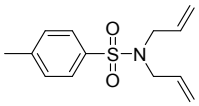

TDA

***N,N*-diallyl-4-methylbenzenesulfonamide (11):** Substrate **11** was synthesized according to the literature procedure.[33]

3. Characterization of ligands

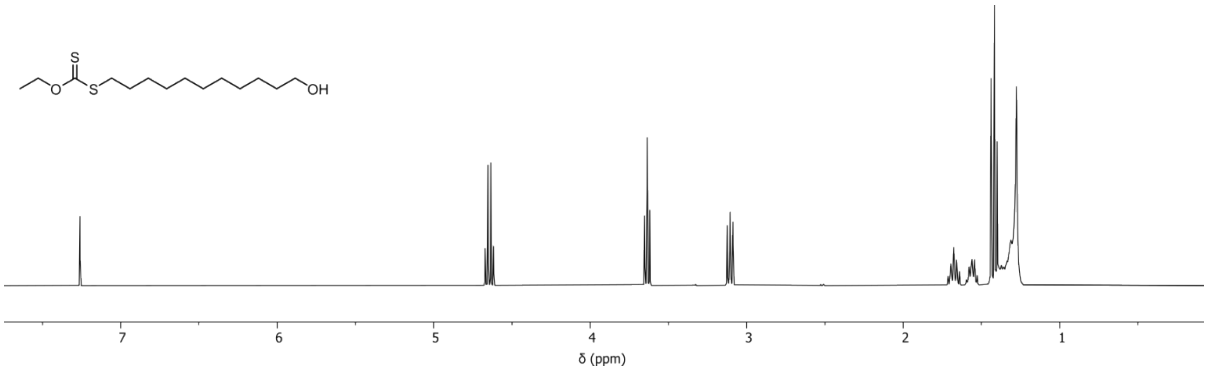

Figure S3. ^{1}H NMR spectrum of **1** in $CDCl_3$, 298 K.

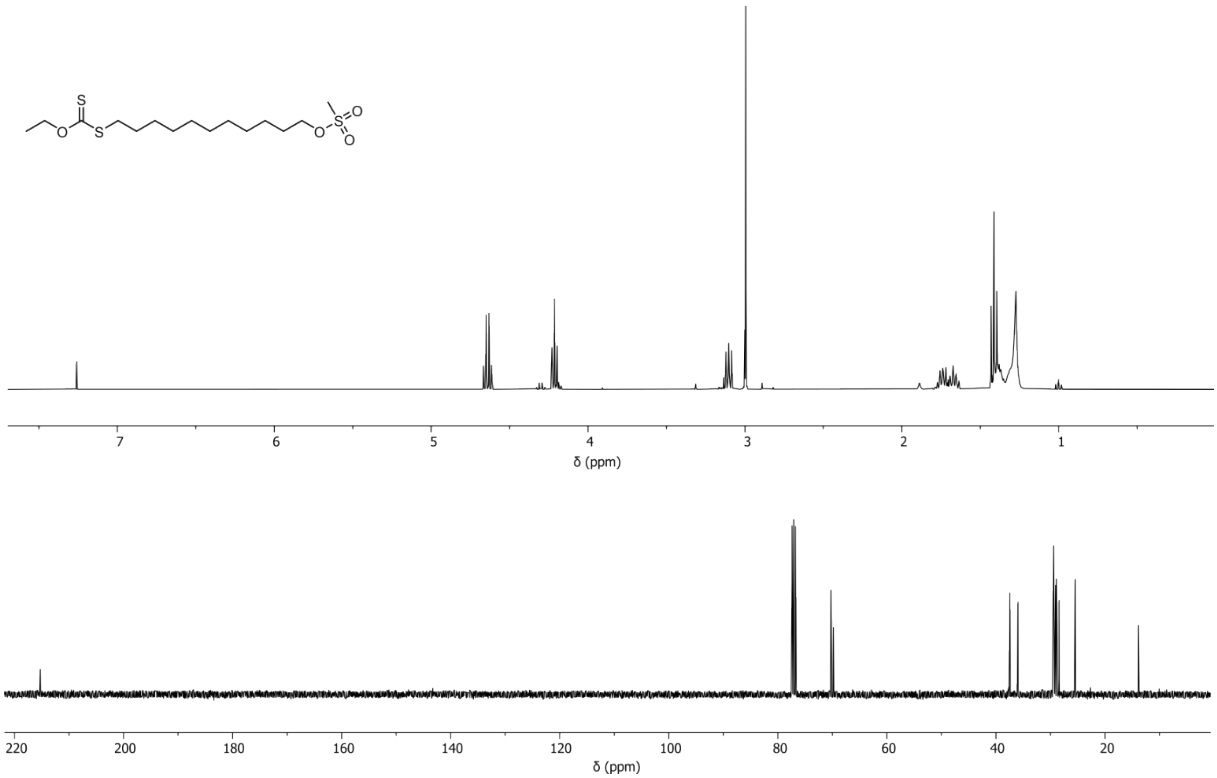

Figure S4. ^{1}H and ^{13}C NMR spectra of **2** in $CDCl_3$, 298 K.

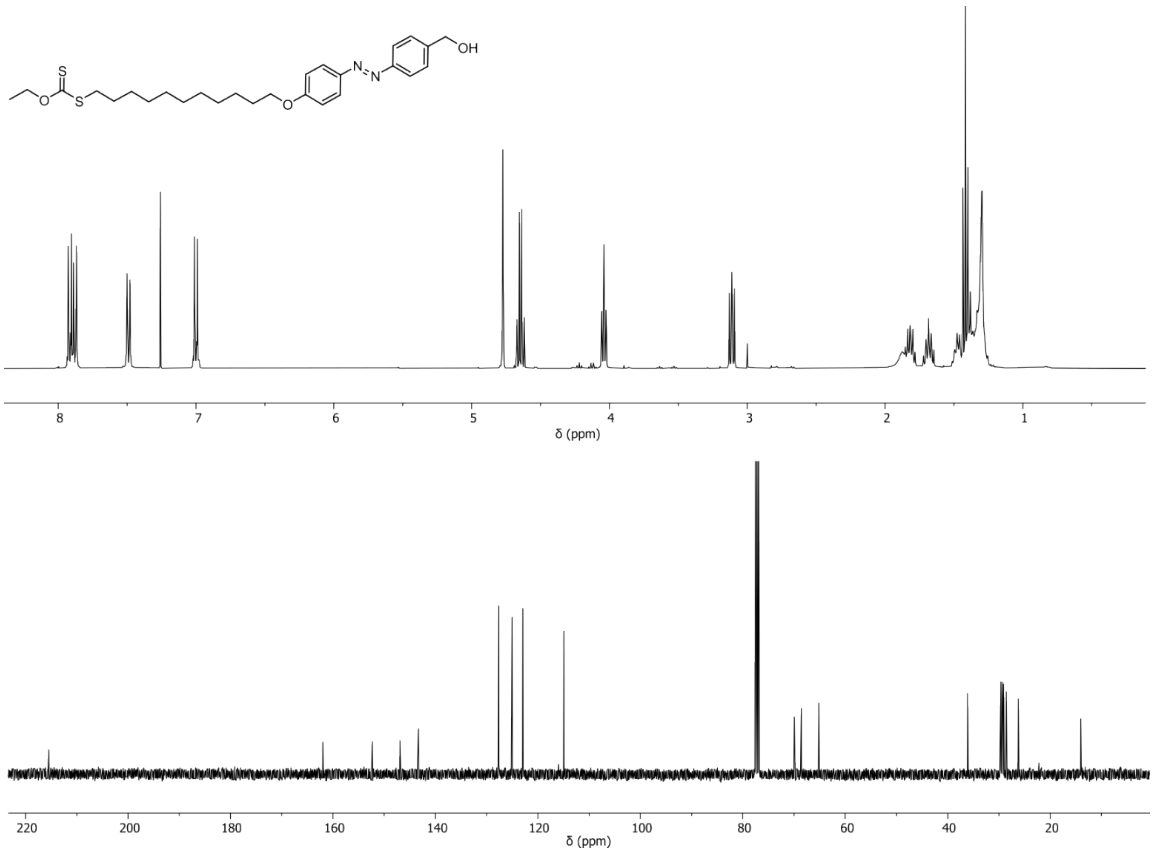

Figure S5. ^{1}H and ^{13}C NMR spectra of **4** in $CDCl_3$, 298 K.

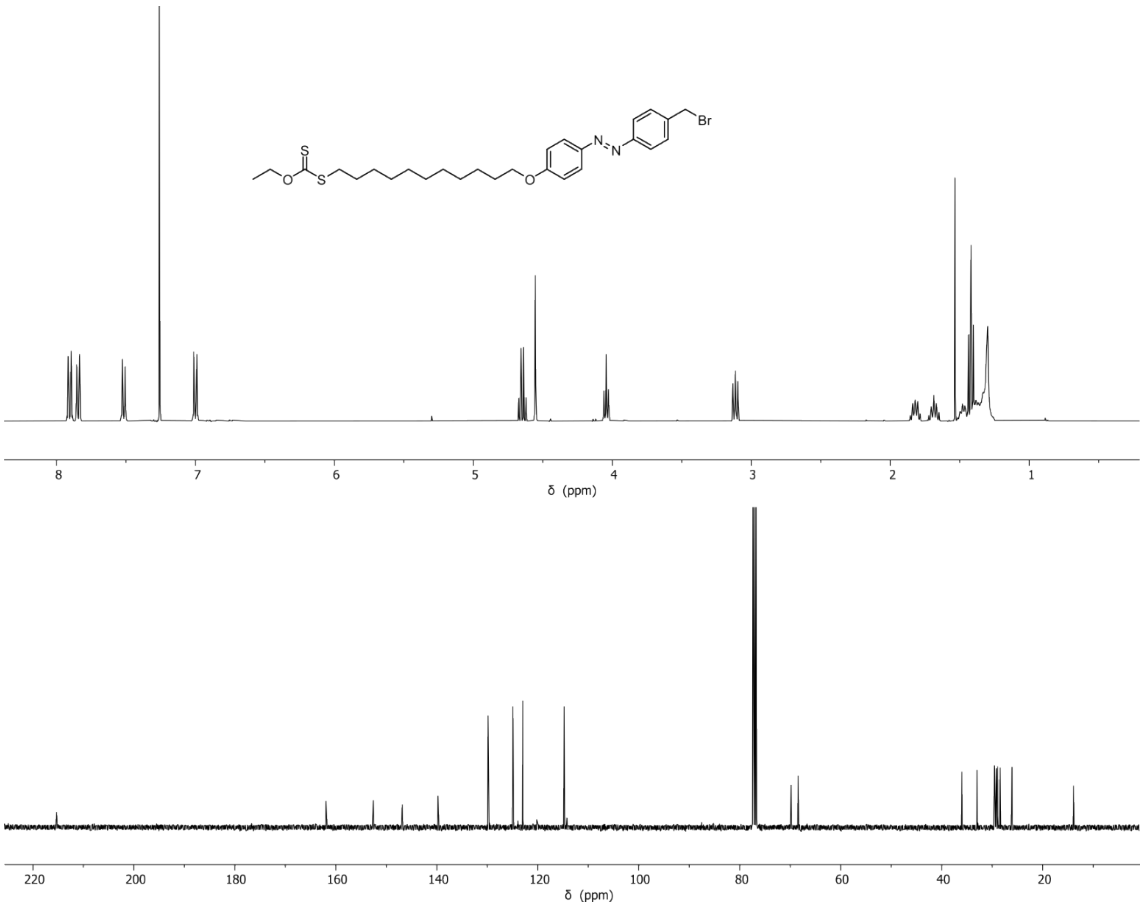

Figure S6. ^{1}H and ^{13}C NMR spectra of **5** in $CDCl_3$, 298 K.

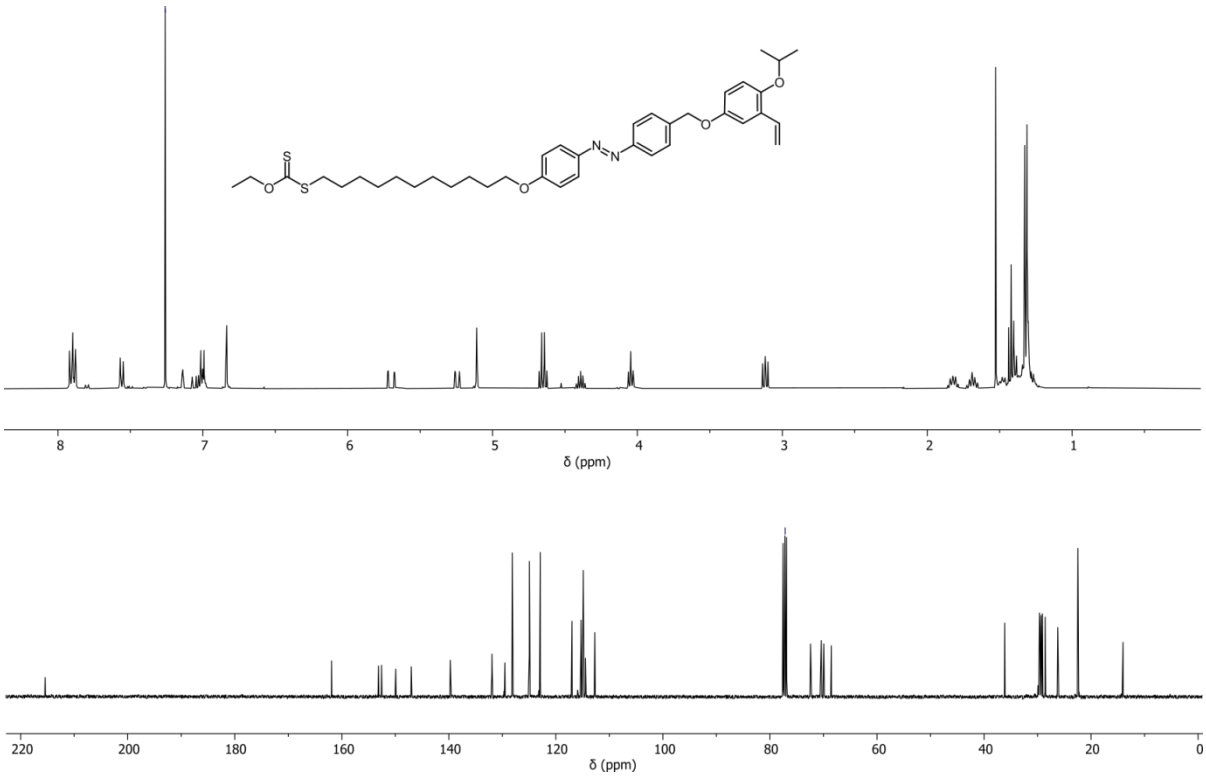

Figure S7. ^{1}H and ^{13}C NMR spectra of **7** in $CDCl_3$, 298 K.

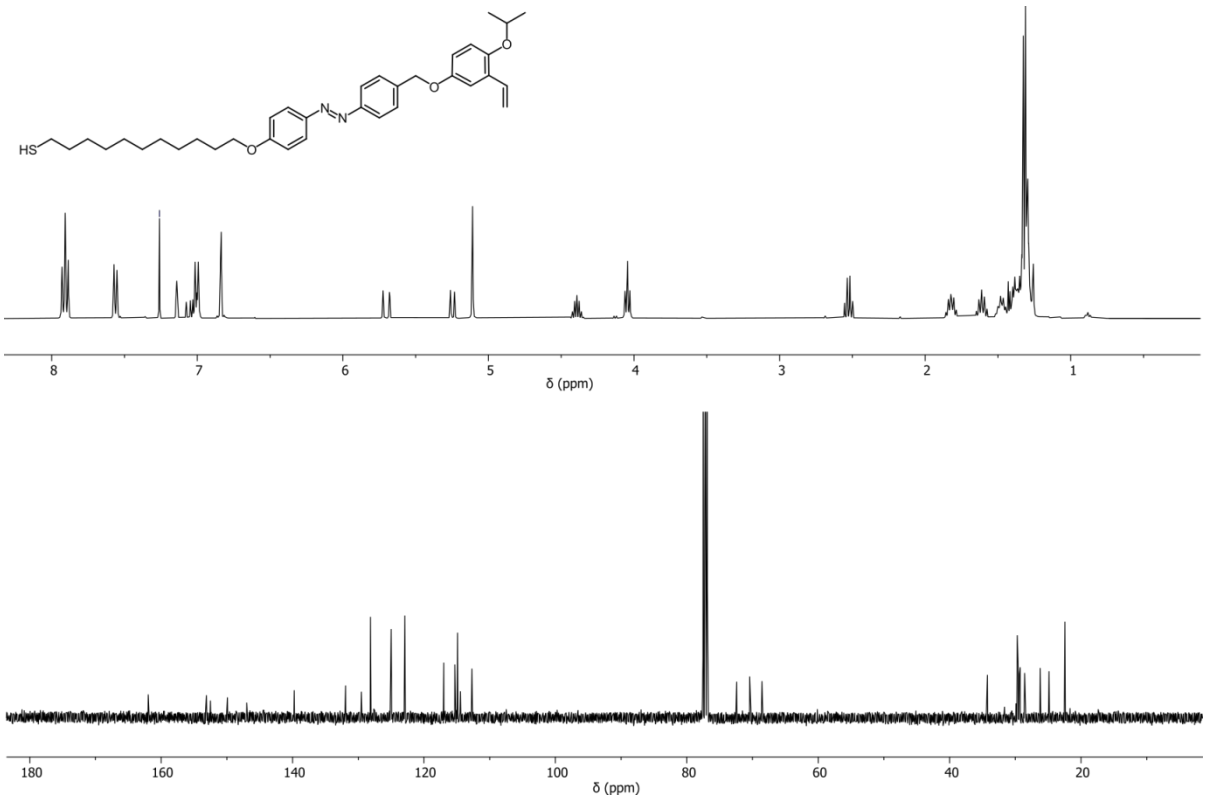

Figure S8. ^{1}H and ^{13}C NMR spectra of **SAT** in $CDCl_3$, 298 K.

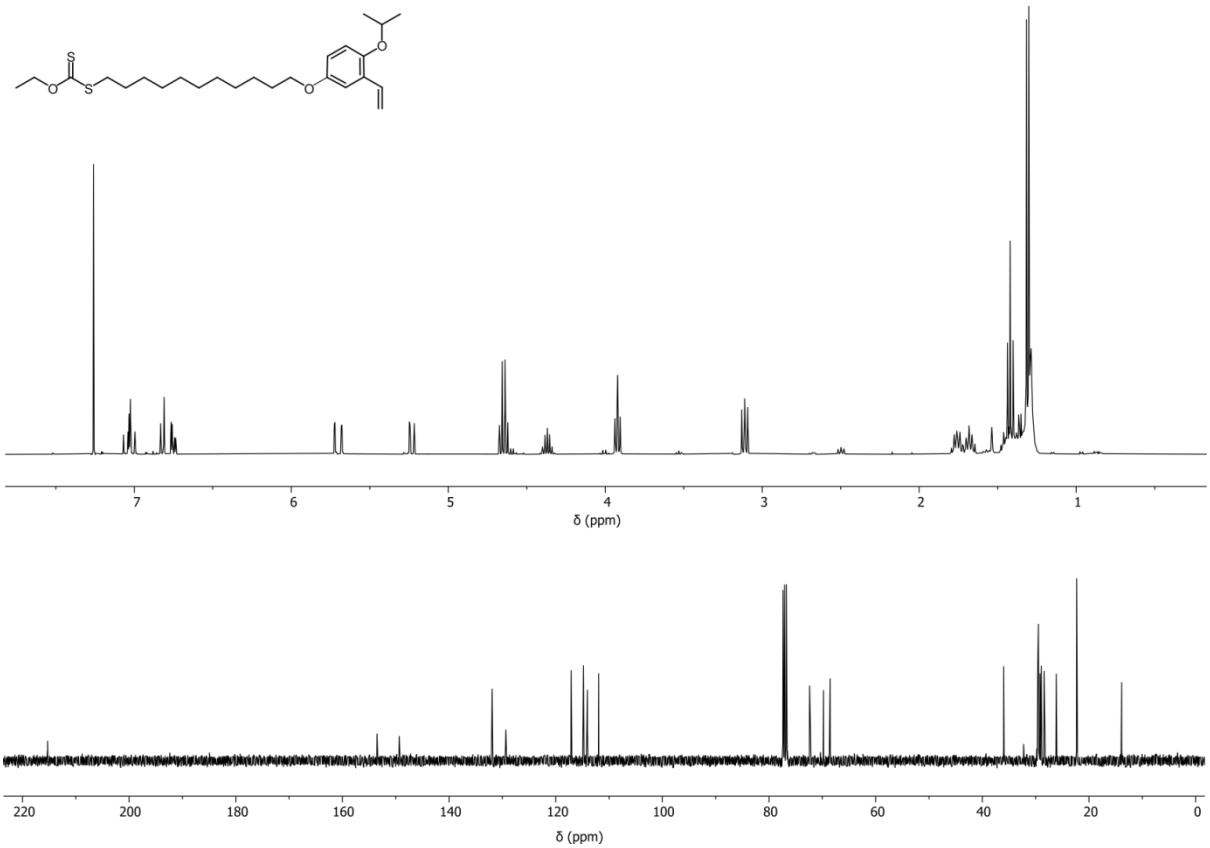

Figure S9. ^{1}H and ^{13}C NMR spectra of **8** in $CDCl_3$, 298 K.

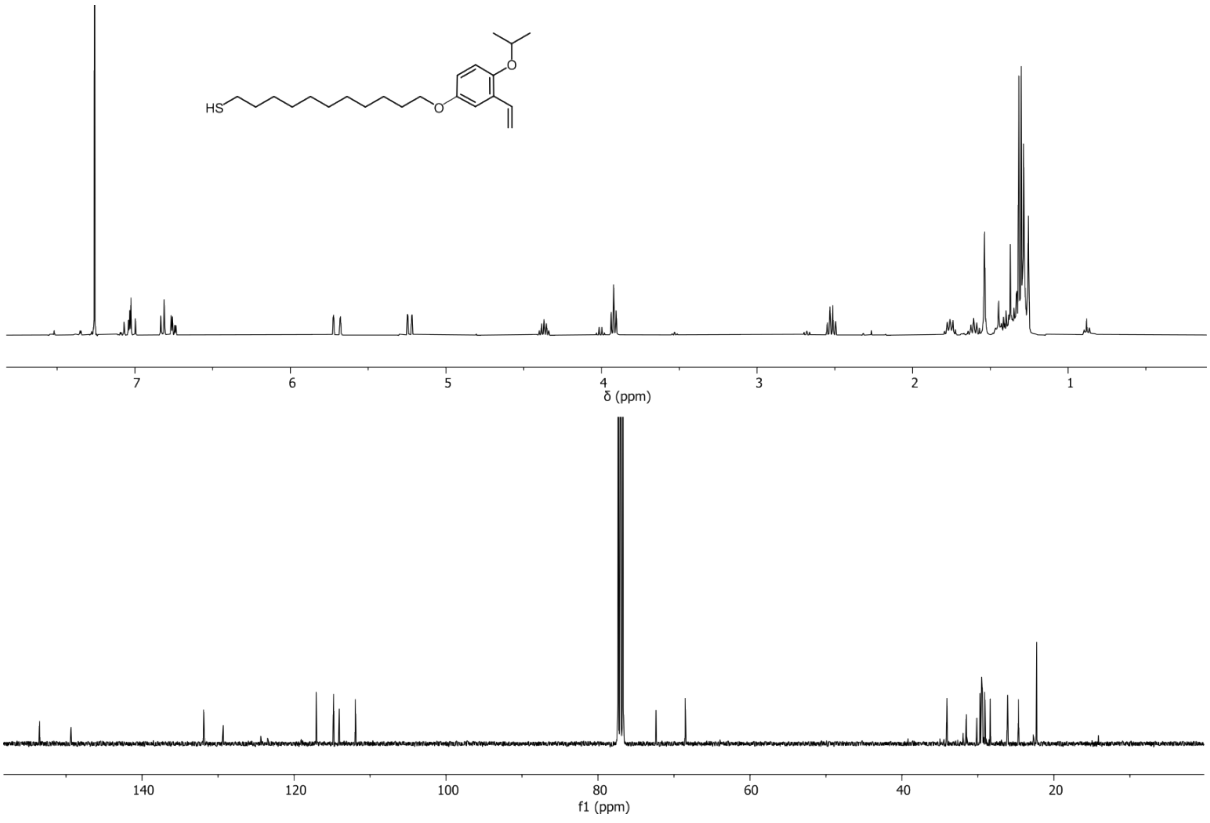

Figure S10. ^{1}H and ^{13}C NMR spectra of **ST** in $CDCl_3$, 298 K.

Elements Used:
C: 0-200 H: 0-200 O: 0-5 S: 1-4 Na: 0-1

Mass	Calc. Mass	mDa	PPM	DBE	Formula	i-FIT	i-FIT Norm	Fit Conf %	C	H	O	S	Na
393.1208	393.1204	0.4	1.0	0.5	C15 H30 O4 S3 Na	712.2	n/a	n/a	15	30	4	3	1

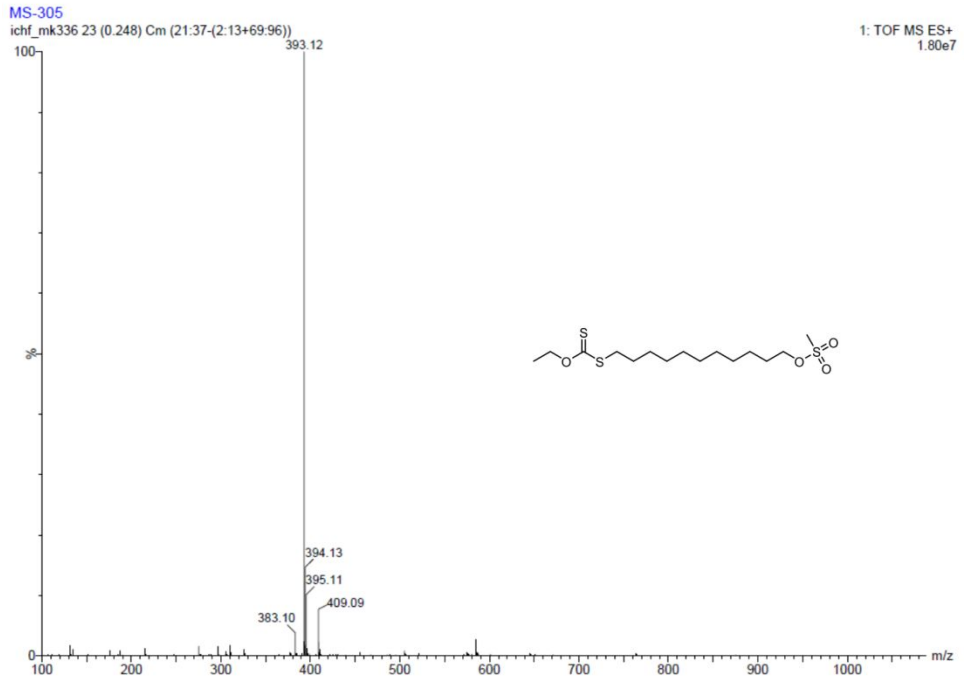

Figure S11. Mass spectrum of **2** under electrospray ionization in positive ion mode.

Elements Used:
C: 0-200 H: 0-200 N: 1-3 O: 0-4 S: 1-3

Mass	Calc. Mass	mDa	PPM	DBE	Formula	i-FIT	i-FIT Norm	Fit Conf %	C	H	N	O	S
503.2398	503.2402	-0.4	-0.8	9.5	C27 H39 N2 O3 S2	576.7	n/a	n/a	27	39	2	3	2

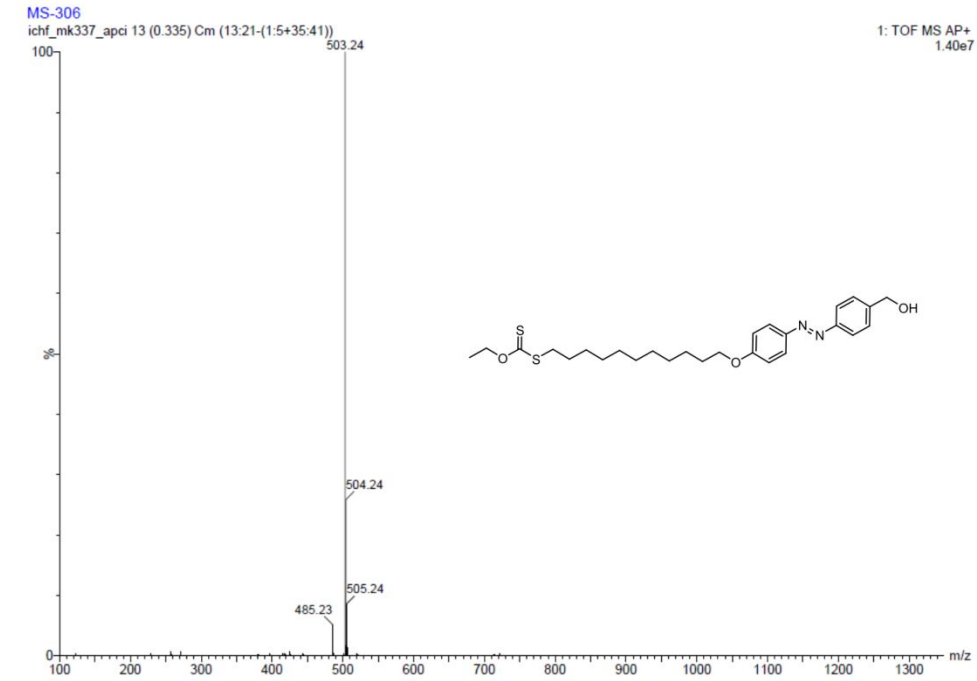

Figure S12. Mass spectrum of **4** under atmospheric pressure chemical ionization in positive ion mode.

Elements Used:
C: 0-200 H: 0-200 N: 0-3 O: 0-3 S: 0-3 Br: 1-2

Mass	Calc. Mass	mDa	PPM	DBE	Formula	i-FIT	i-FIT Norm	Fit Conf %	C	H	N	O	S	Br
565.1561	565.1558	0.3	0.5	9.5	C27 H38 N2 O2 S2 Br	484.0	0.021	97.96	27	38	2	2	2	1
	565.1565	-0.4	-0.7	18.5	C35 H34 S Br	487.8	3.892	2.04	35	34			1	1

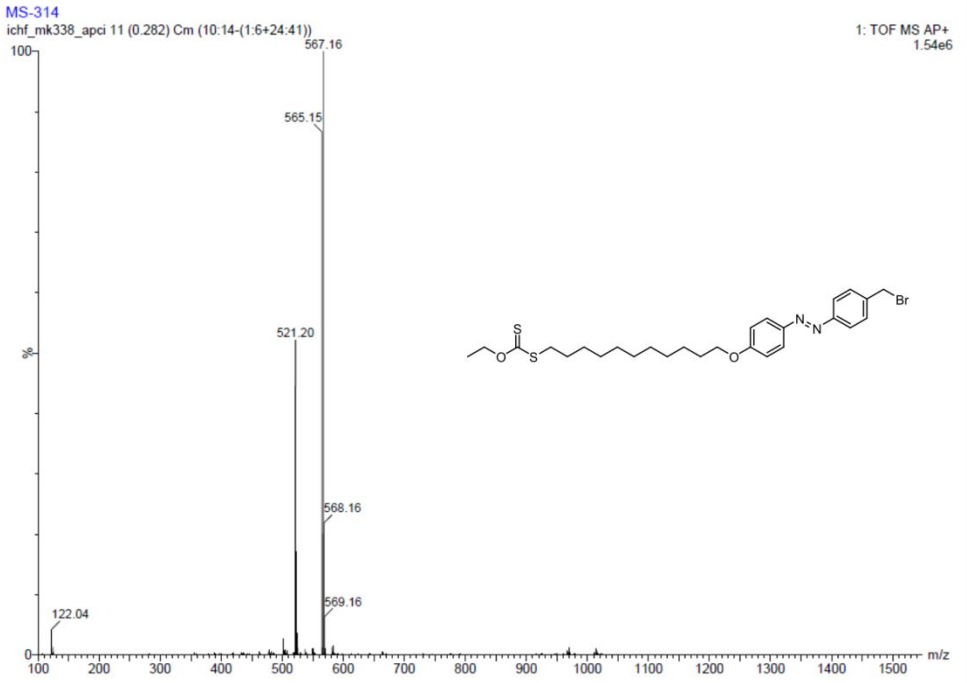

Figure S13. Mass spectrum of **5** under atmospheric pressure chemical ionization in positive ion mode.

Elements Used:
C: 0-200 H: 0-200 N: 0-3 O: 0-5 S: 0-3

Mass	Calc. Mass	mDa	PPM	DBE	Formula	i-FIT	i-FIT Norm	Fit Conf %	C	H	N	O	S
663.3289	663.3290	-0.1	-0.2	14.5	C38 H51 N2 O4 S2	410.1	0.002	99.82	38	51	2	4	2
	663.3297	-0.8	-1.2	23.5	C46 H47 O2 S	416.4	6.324	0.18	46	47		2	1

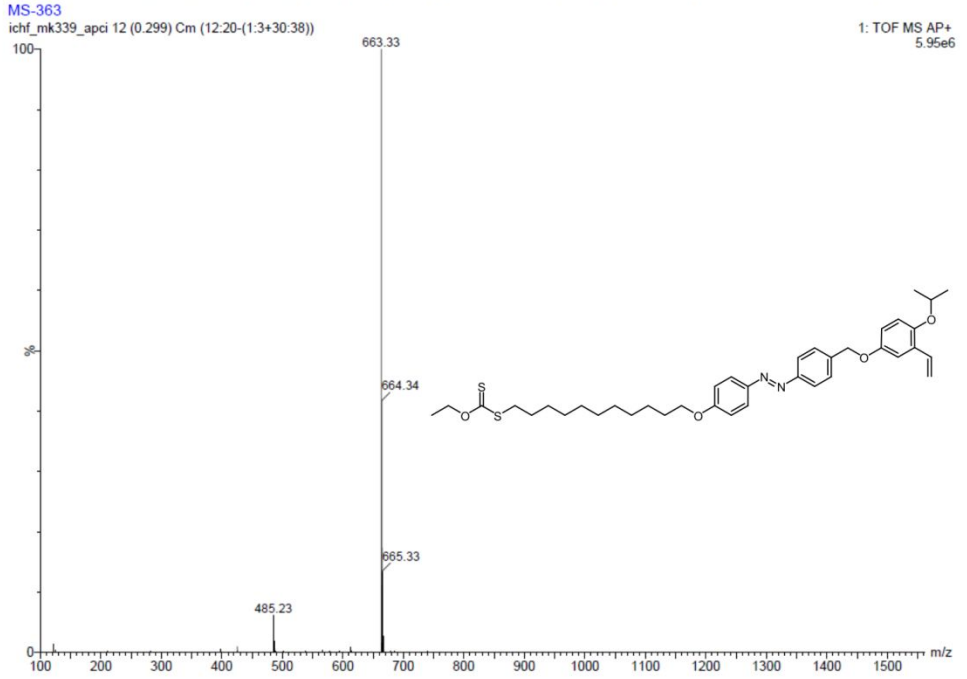

Figure S14. Mass spectrum of **7** under atmospheric pressure chemical ionization in positive ion mode.

Elements Used:
C: 0-100 H: 0-200 N: 0-2 O: 0-6 S: 0-1

Mass	Calc. Mass	mDa	PPM	DBE	Formula	i-FIT	i-FIT Norm	Fit Conf %	C	H	N	O	S
575.3309	575.3307	0.2	0.3	13.5	C35 H47 N2 O3 S	226.1	0.000	99.99	35	47	2	3	1
	575.3314	-0.5	-0.9	22.5	C43 H43 O	235.8	9.635	0.01	43	43		1	

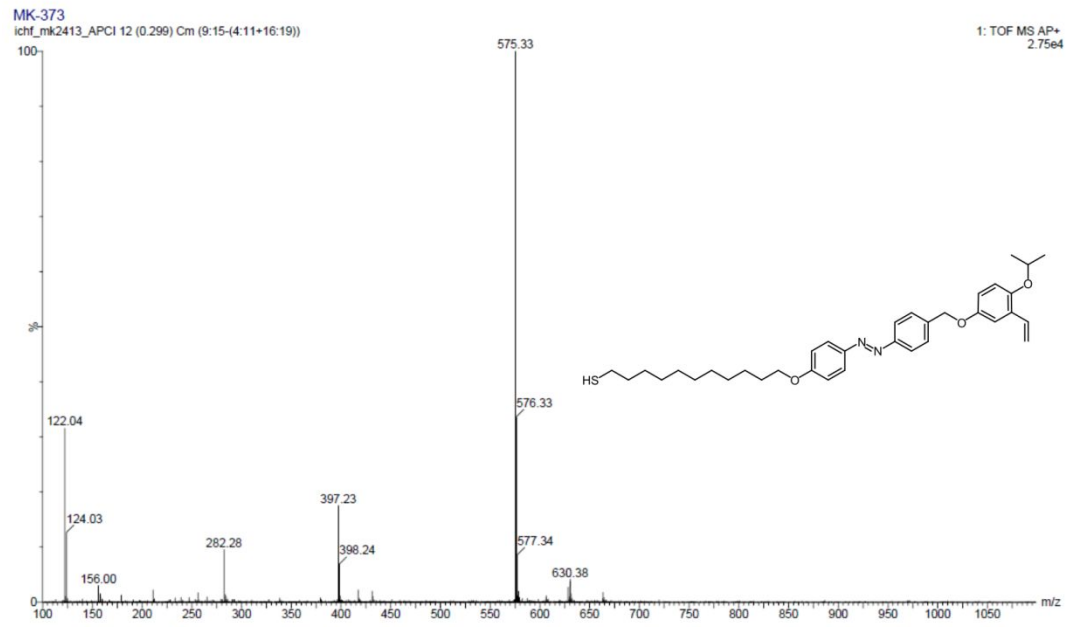

Figure S15. Mass spectrum of **SAT** under electrospray ionization in positive ion mode.

Elements Used:
C: 0-150 H: 0-200 N: 0-1 O: 0-6 Na: 0-1 S: 1-2

Mass	Calc. Mass	mDa	PPM	DBE	Formula	i-FIT	i-FIT Norm	Fit Conf %	C	H	N	O	Na	S
475.2318	475.2317	0.1	0.2	5.5	C25 H40 O3 Na S2	825.8	0.001	99.86	25	40		3	1	2

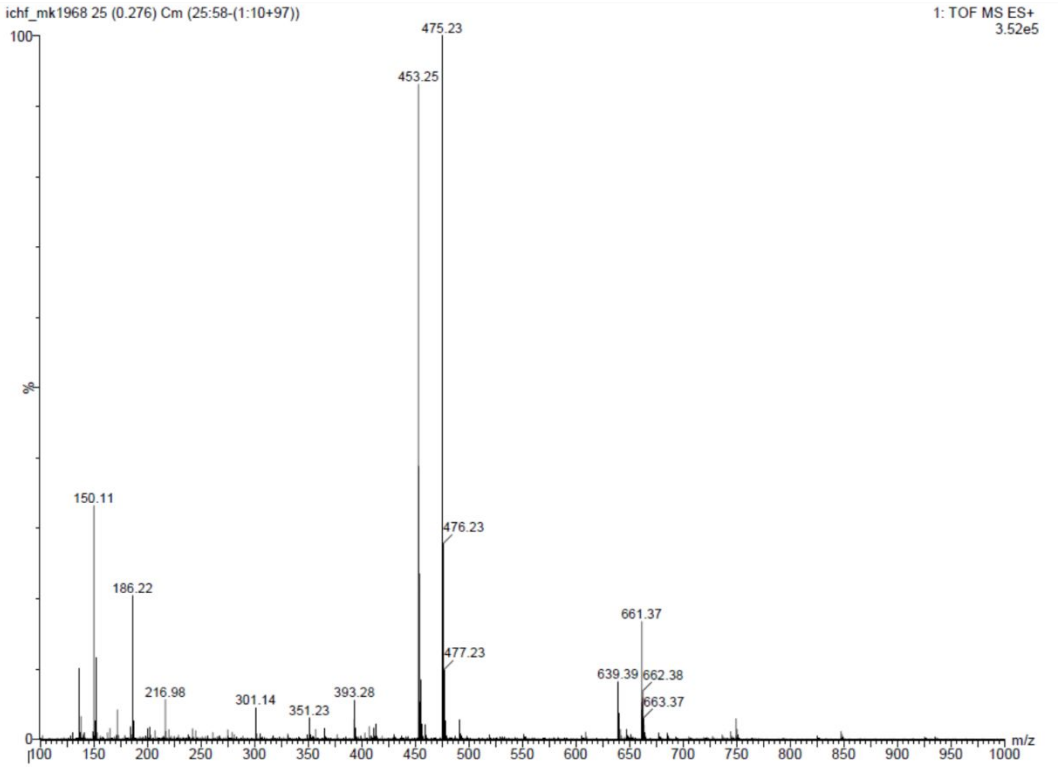

Figure S16. Mass spectrum of **8** under electrospray ionization in positive ion mode.

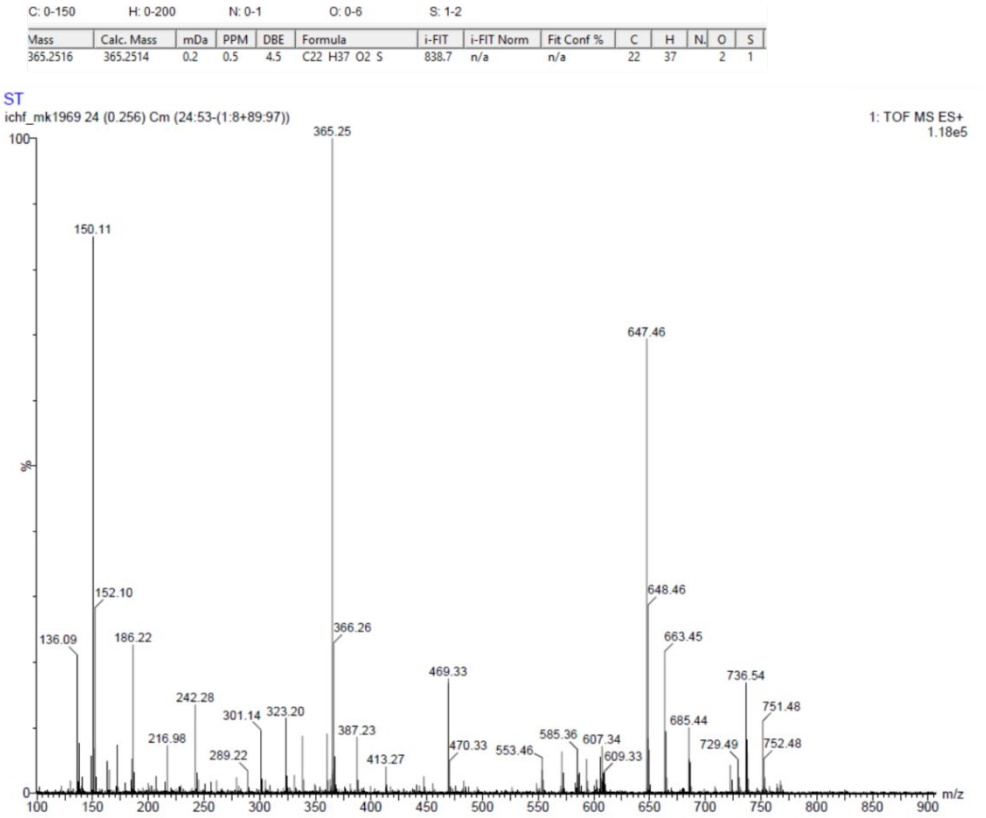

Figure S17. Mass spectrum of **ST** under electrospray ionization in positive ion mode.

4. Synthesis and functionalization of AuNPs

Synthesis of thiol-coated AuNPs

$HAuCl_4 \cdot 3H_2O$ (2.4 mg, 6 μmol) was dissolved in the presence of dodecylamine (21.6 mg) in 0.6 mL of 0.1M didocelydimethylammonium bromide (DDAB) toluene solution and then reduced by tetrabutylammonium borohydride (6 mg dissolved in 0.24 ml of 0.1M DDAB toluene solution) added in one portion under vigorous stirring. The resulting mixture was stirred for 1h. Then, the prescribed amount of SAT or ST and PT or HDT (total number of moles: 1.8 μmol) in DCM (200 μL) was added in one portion, and the resulting mixture was stirred for 1h.

Purification of χSAT(PT)@AuNPs and χST(PT)@AuNPs

PT-containing NPs were precipitated by pouring the reaction mixture into MeOH (6 mL) and collected by centrifugation. The NP precipitate was redispersed in $CHCl_3$ (80 μL), precipitated by MeOH (6 mL) and centrifuged. The procedure was repeated two times. For the third time, the NPs were redispersed in $CHCl_3$ (80 μL), precipitated with pentane (7 mL) and centrifuged. Finally, the NP sediment was dried and redispersed in 400 μL of deuterated DCM to give 7 mM (in terms of gold) NP dispersion.

Purification of χSAT(HDT)@AuNPs

HDT-containing NPs were precipitated by pouring the reaction mixture into MeOH (6 mL) and collected by centrifugation. The NP precipitate was redispersed in $CHCl_3$ (80 μL), precipitated by MeOH (6 mL) and centrifuged. The procedure was repeated two times. For the third time, the

NPs were redispersed in 80 µL of $CHCl_3$-pentane mixture (1:1 *v/v*), precipitated with acetone (7 mL) and centrifuged. Finally, the NP sediment was dried and redispersed in 400 µL of deuterated DCM to give 7 mM (in terms of gold) NP dispersion.

Generation of Ru precatalyst
To a stirred solution of χSAT(PT)@AuNPs (7 mM) or χSAT(HDT)@AuNPs (7 mM) or χST(PT)@AuNPs (7 mM) in 400 µL of deuterated DCM was added Grubbs catalyst 2nd generation (0.18 mg, 0.21 µmol) in 100 µL of deuterated DCM, and copper(I) chloride (0.02 mg, 0.21 µmol), and the resulting mixture was stirred for 2h. Final NPs were used in metathesis reaction without any purification.

5. Characterization of AuNPs

Sample preparation for TEM
20SAT(PT)@AuNPs and 20SAT(PT)Ru@AuNPs dispersions were dropcasted on 300 mesh Cu grids and used for further analysis.

Sample preparation for TGA
20SAT(PT)@AuNPs and PT@AuNPs dispersions were transferred to ceramic crucibles, dried and used for further analysis.

Sample preparation for XPS
A 500 µL dispersion of 20SAT(PT)Ru@AuNPs (7 µM) in DCM was concentrated under vacuum, redispersed in DCM (80 µL) and precipitated with pentane (7 mL). The procedure was repeated three times. Finally, the NP sediment was washed twice with methanol (10 mL), dried and dispersed in 80 µL of DCM. The resultant NP dispersion was dropcasted on a silicon wafer and used for further analysis.

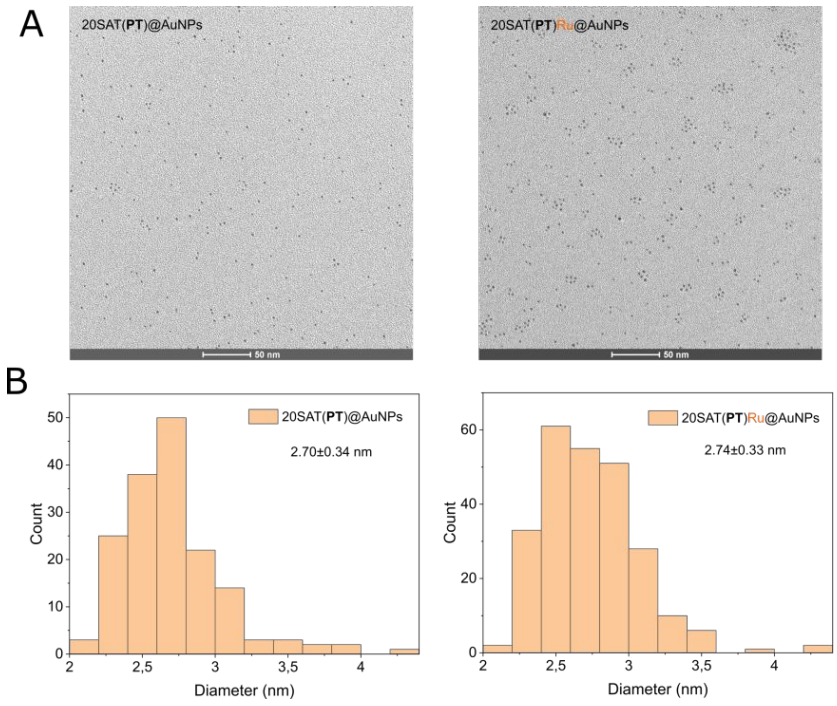

Figure S18. TEM micrographs and size analysis of 20SAT(PT)@AuNPs before and after the reaction with **G2**.

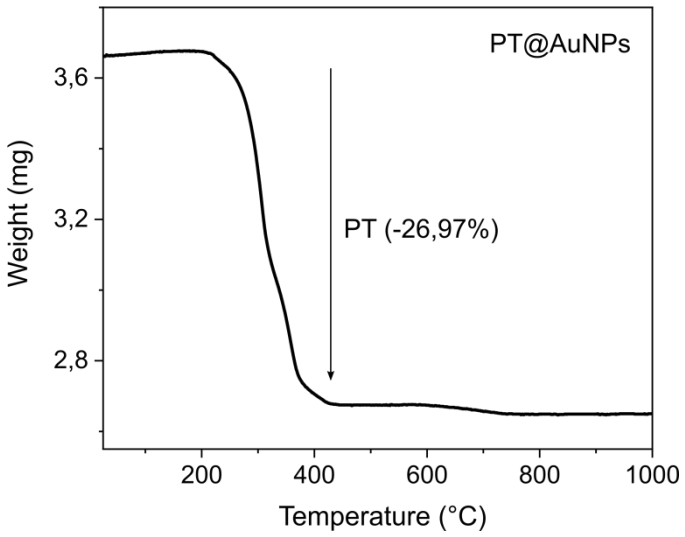

Figure S19. Thermograms of AuNPs coated with neat PT (A) and HDT (B) monolayers.

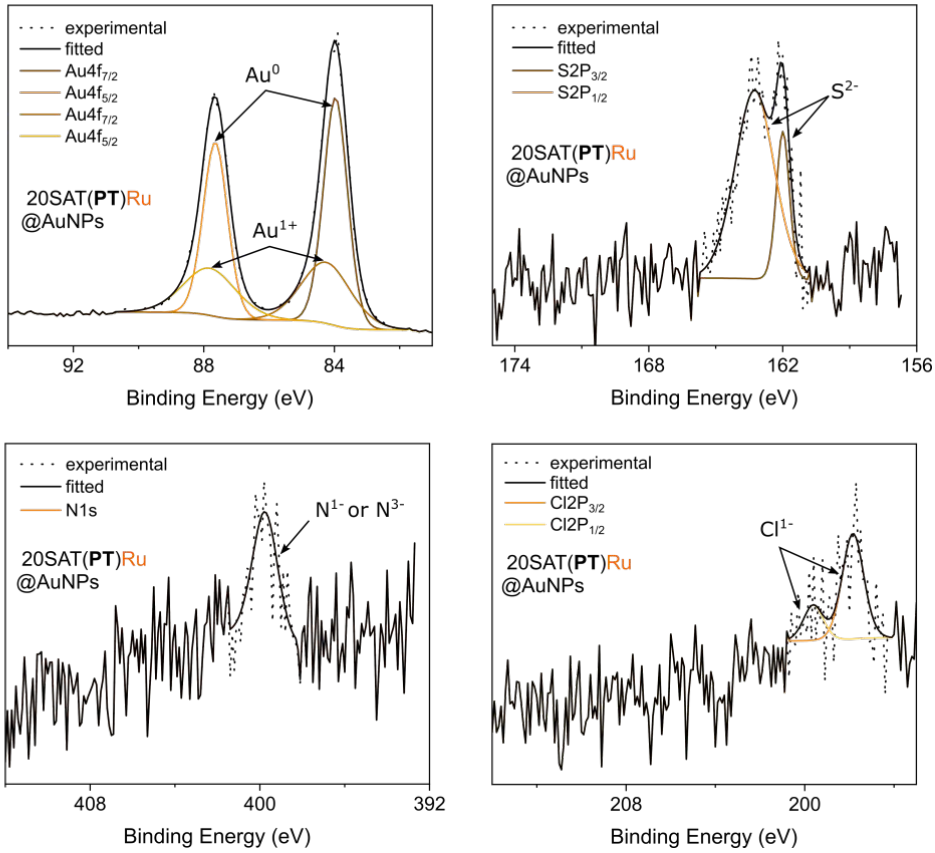

Figure S20. XPS spectra of 20SAT(PT)Ru@AuNPs revealing the presence of: (i) neutral and oxidized gold, indicating the presence of gold nanoparticles and the thiol monolayer on their surface; (ii) reduced sulphur, which is another proof for adsorbed thiolates; (iii) reduced nitrogen, indicative of the presence of azo bond/NHC ligand; (iv) reduced chlorine, which is an additional indication of the presence of **H2** moiety.

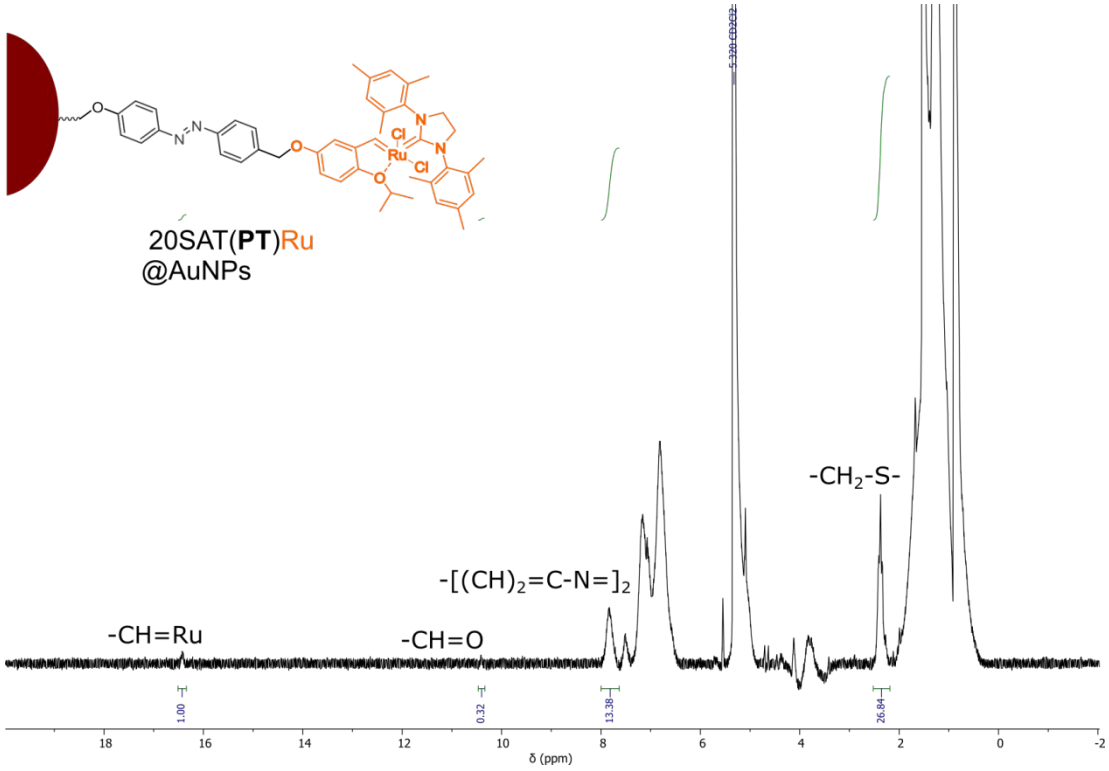

Figure S21. Full ^{1}H NMR spectrum of 20SAT(PT)Ru@AuNPs with indicated proton resonances integrated to determine the ratio between SAT and PT ligands and the percentage of SAT reacted with **G2**, DCM-d_2, 298 K.

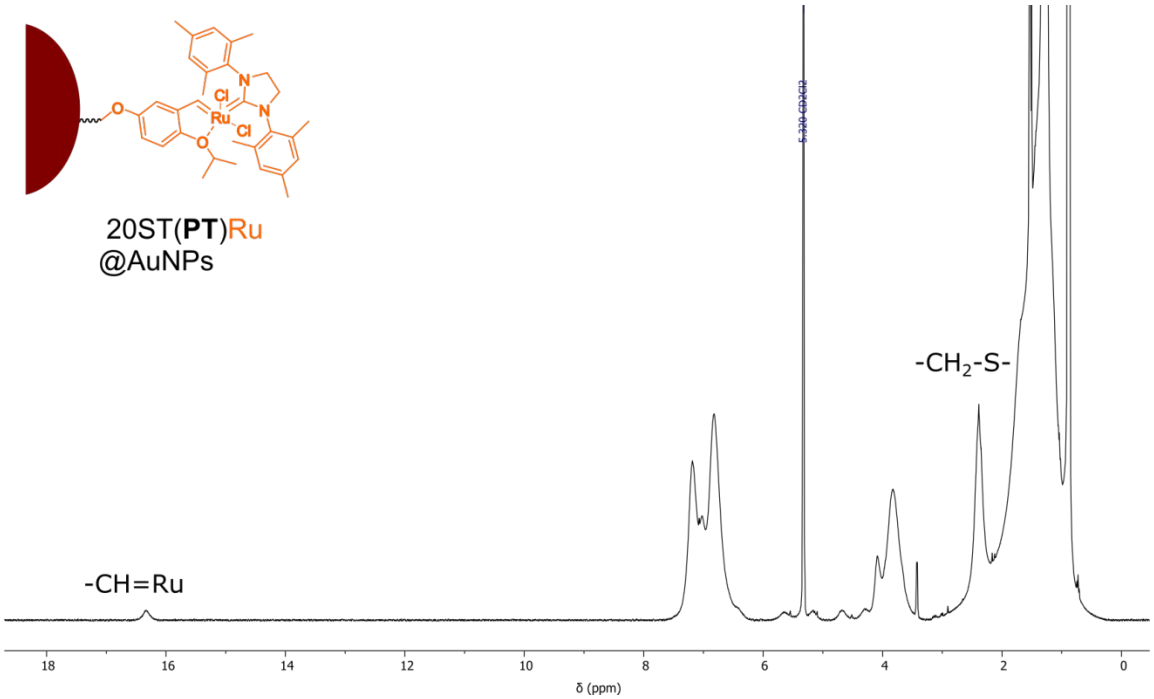

Figure S22. ^{1}H NMR spectrum of 20ST(PT)Ru@AuNPs, DCM-d_2, 298 K.

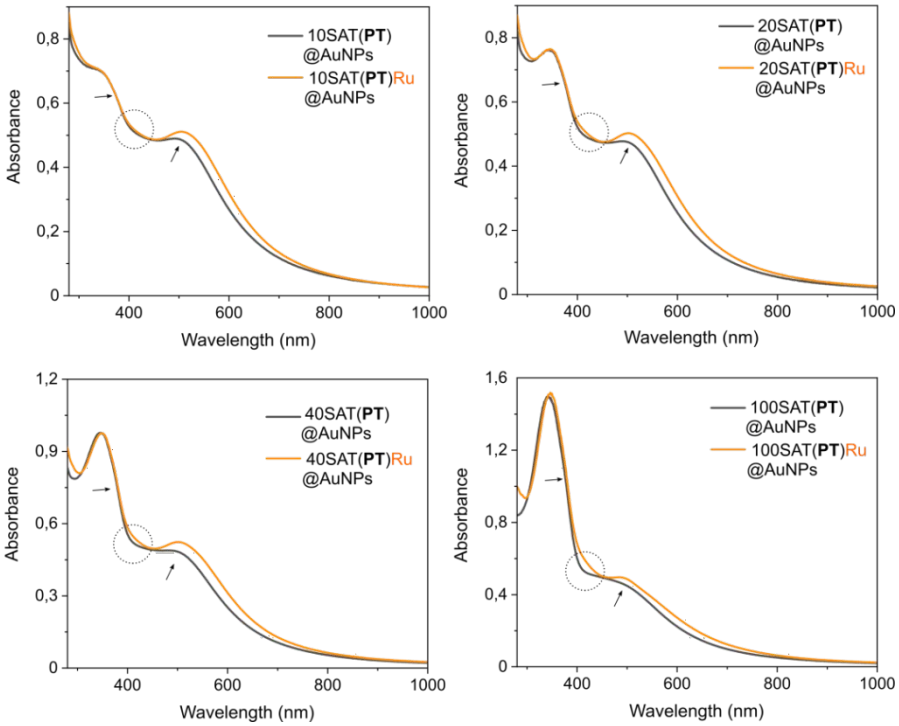

Figure S23. Normalized absorbance spectra of AuNPs coated with SAT and PT ligands in different ratios before and after agitating with **G2** for 2h.

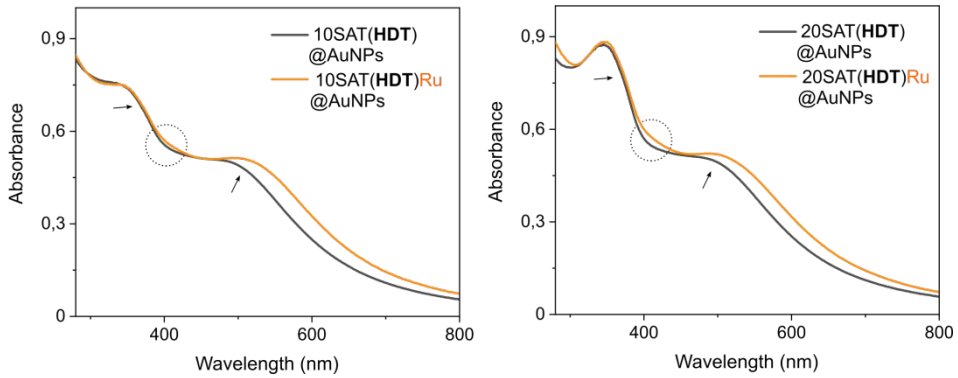

Figure S24. Normalized absorbance spectra of AuNPs coated with SAT and HDT ligands in different ratios before and after agitating with **G2** for 2h.

6. Isomerization experiments

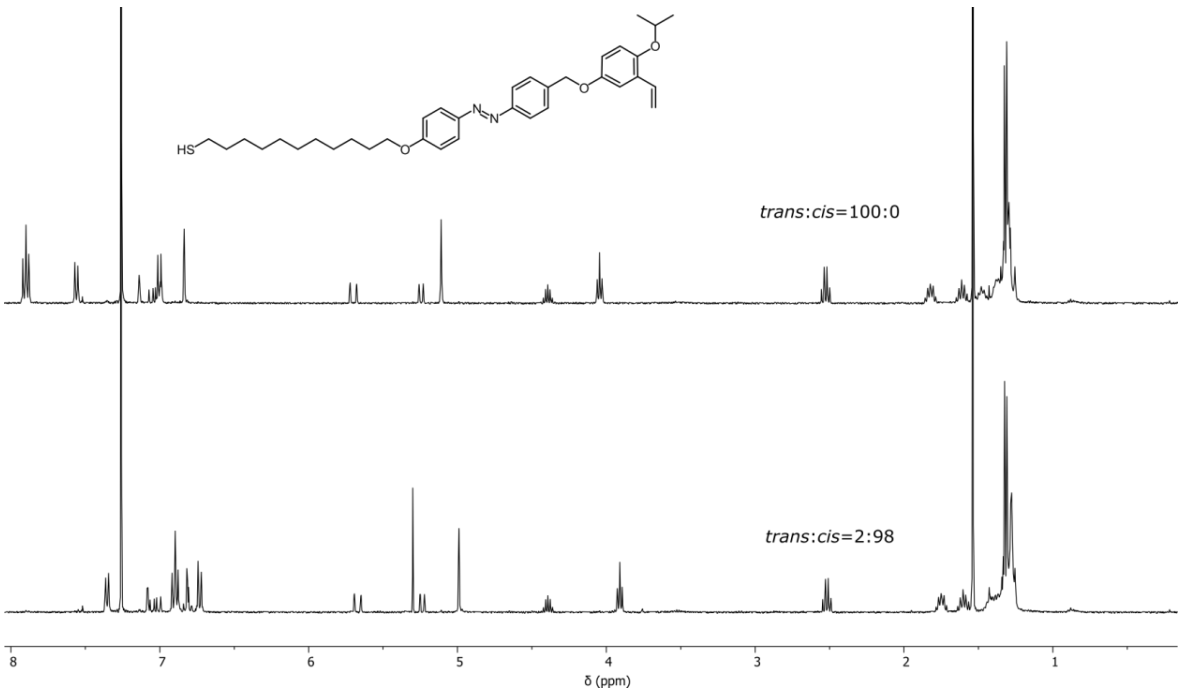

Figure S25. ^{1}H NMR spectra of SAT (1.1 mM) in the dark (top) and after being irradiated with 365 nm for 30 min (bottom) showing only the traces of the *cis* isomer in the photostationary state, $CDCl_3$, 298 K.

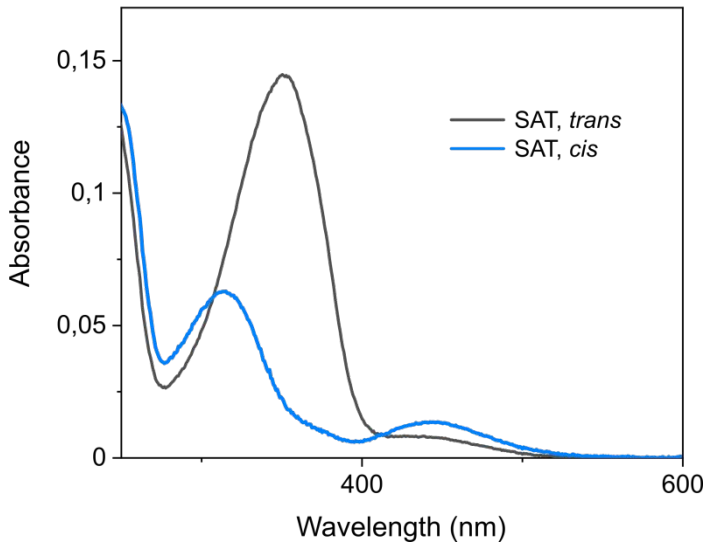

Figure S26. Absorbance spectra of SAT (0.006 mM) in the dark and after being irradiated with 365 nm for 2 min in DCM, 298 K.

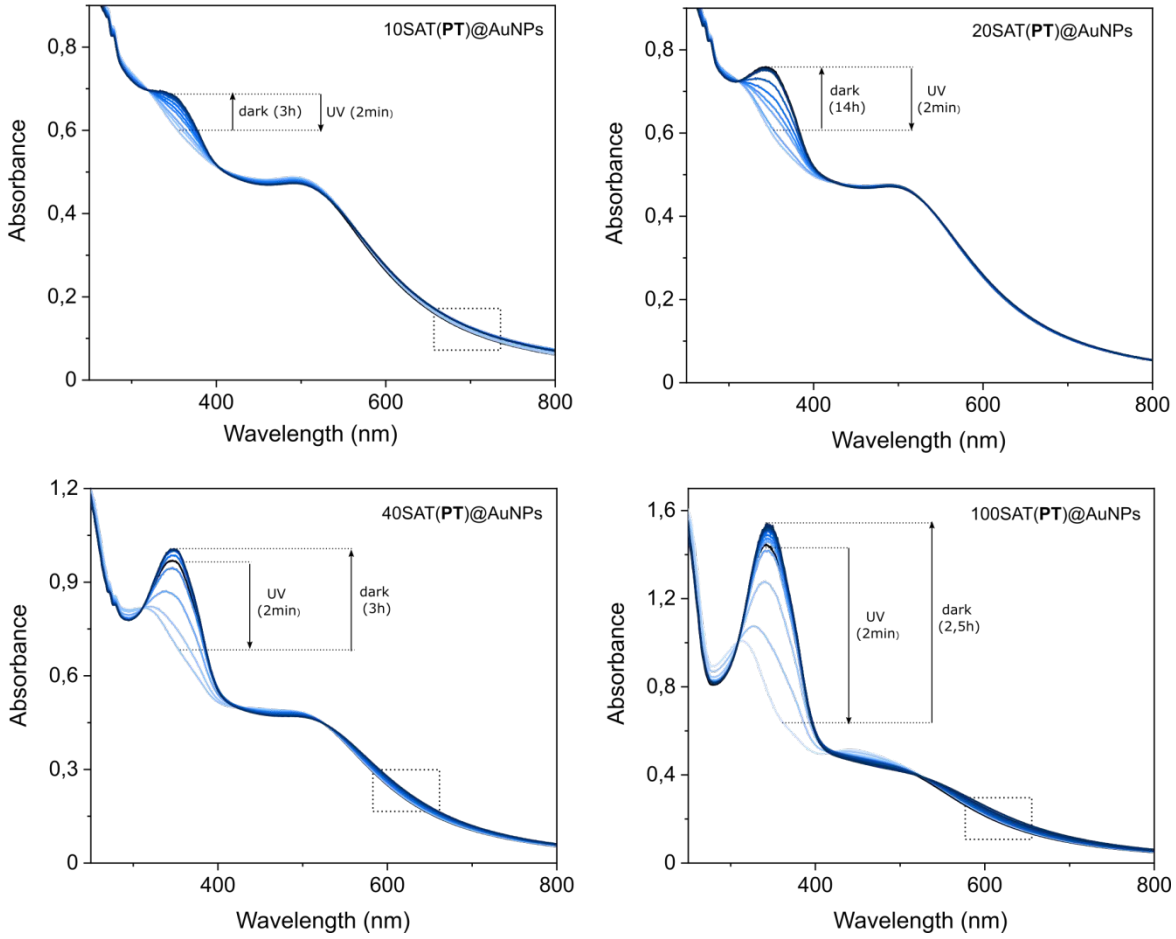

Figure S27. Normalized absorbance spectra of SAT/PT coated AuNPs (0.14 mM) in DCM in their initial states, after irradiation with 365 nm light and under thermal relaxation in the dark. The increase in the intensity of the π-π* band and the broadening of the plasmon peak indicate the aggregation of AuNPs.

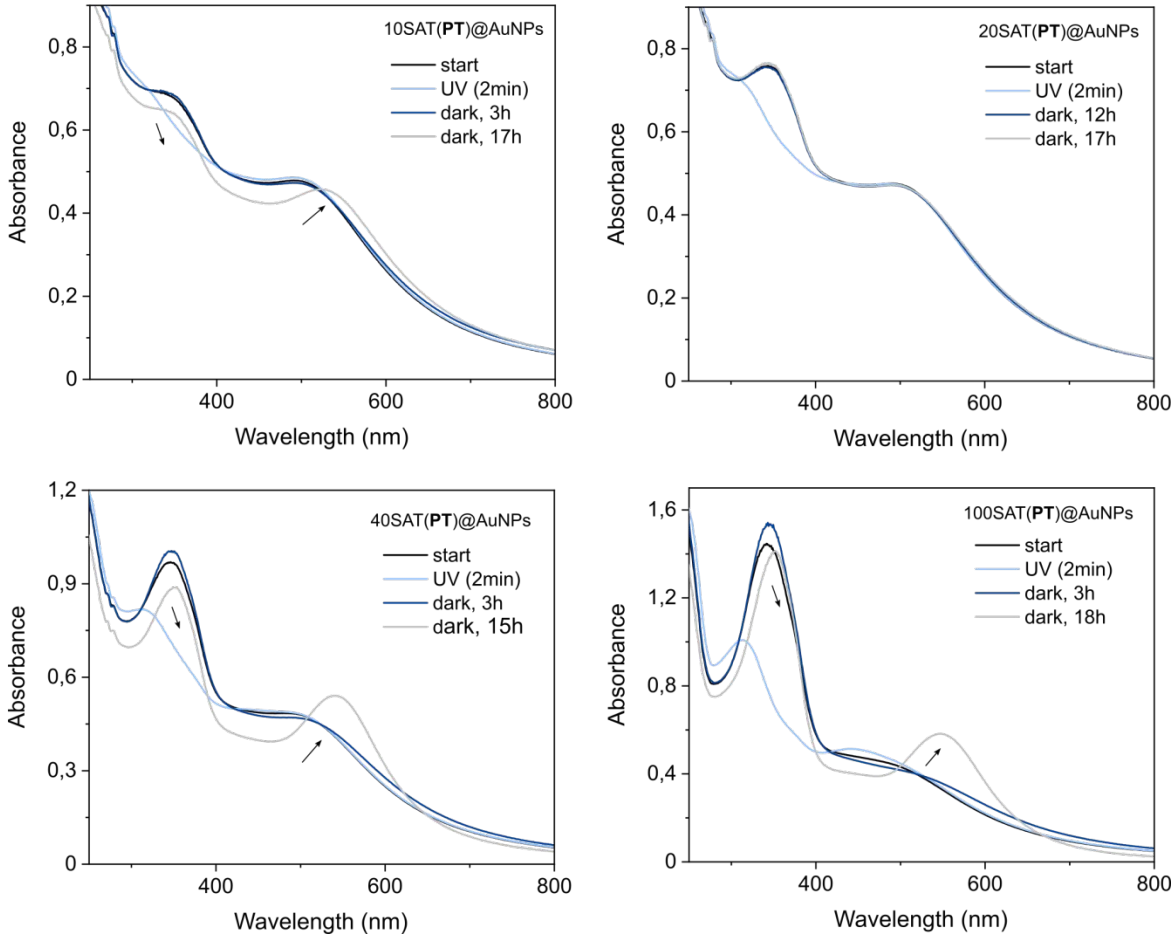

Figure S28. Normalized absorbance spectra of SAT/PT coated AuNPs (0.14 mM) in DCM kept after irradiation in the dark overnight. The decrease in intensity and appearance of a new broad peak indicate further aggregation and sedimentation of AuNPs, visible to the naked eye as a color change from red-brown to dark violet.

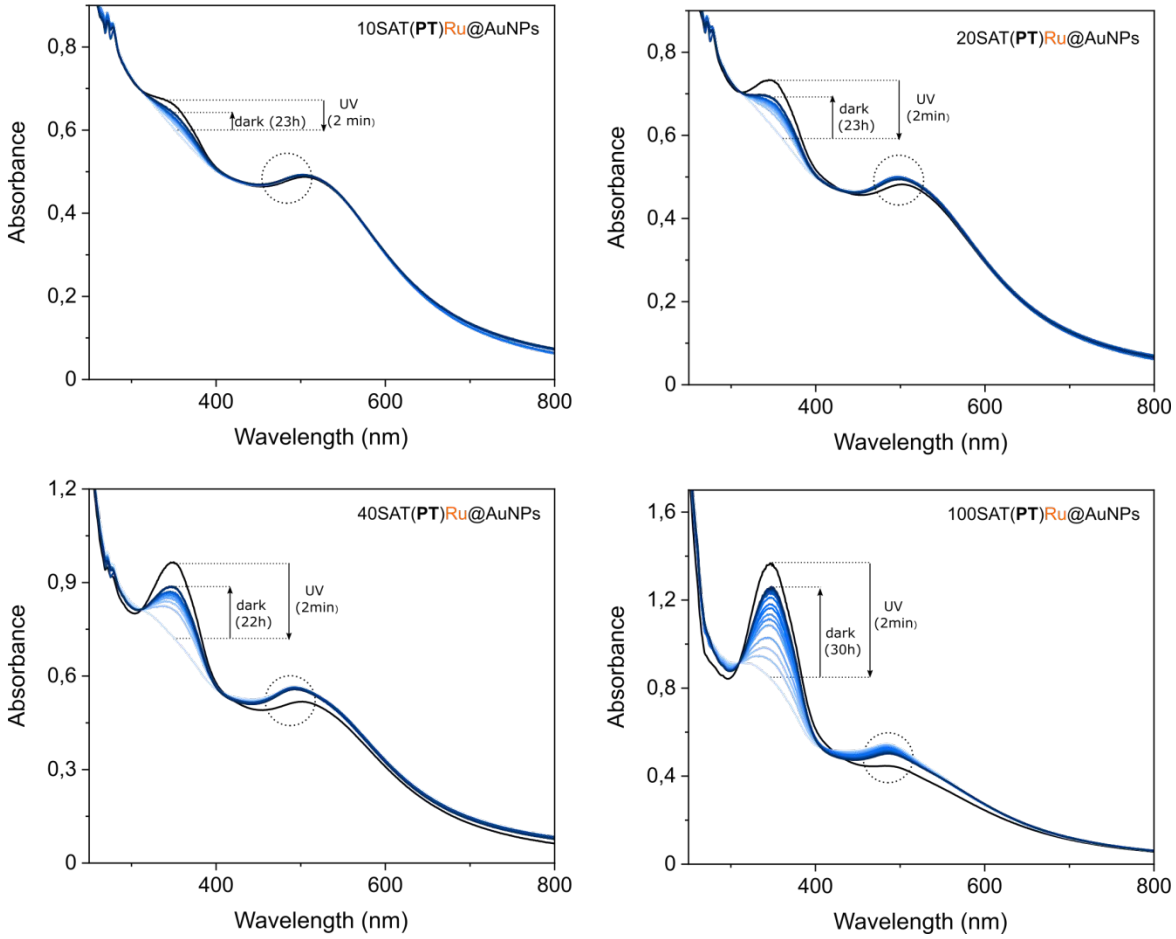

Figure S29. Normalized absorbance spectra of SAT/PT/Ru coated AuNPs (0.14 mM) in DCM in their initial states, after irradiation with 365 nm light and under thermal relaxation in the dark. The appearance of a new peak around 500 nm during irradiation, which does not disappear in the dark, indicates a strong interaction between the metalated SAT ligand and the surrounding monolayer.

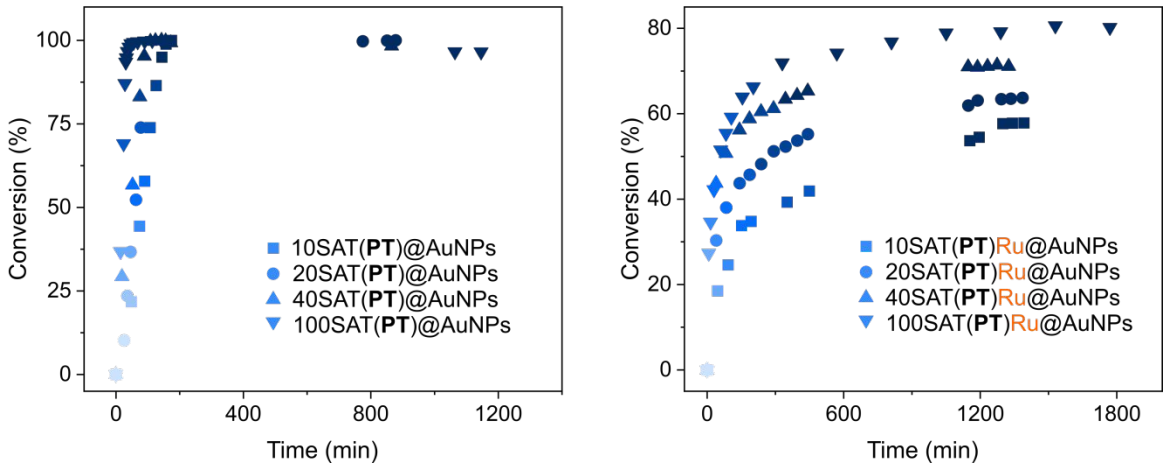

Figure S30. Comparative kinetics of the back isomerization of SAT/PT coated AuNPs without and with Ru.

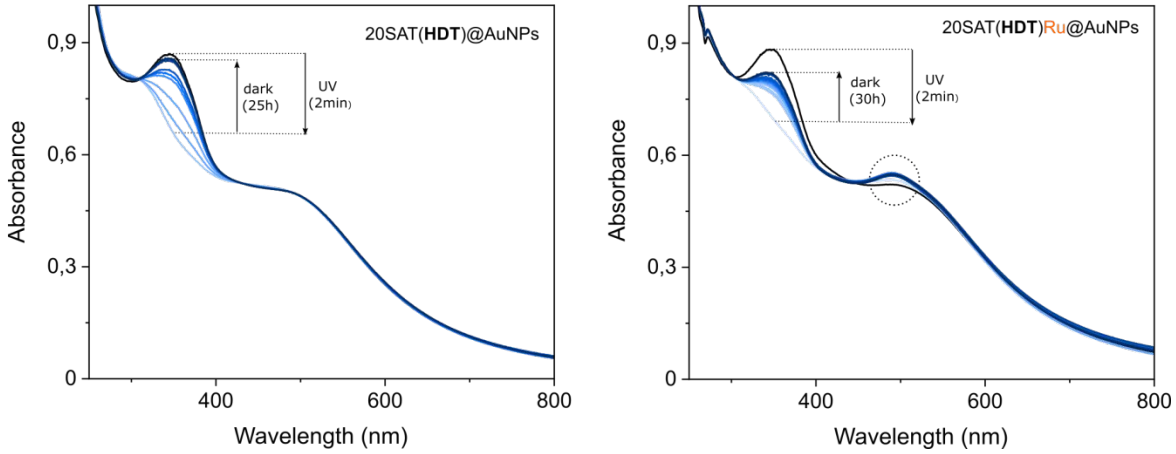

Figure S31. Normalized absorbance spectra of 20SAT(HDT)@AuNPs without and with Ru (0.14 mM) in DCM in their initial states, after irradiation with 365 nm light and under thermal relaxation in the dark. Similar to PT containing AuNPs, the irreversible appearance of a new peak around 500 nm was observed in the presence of Ru.

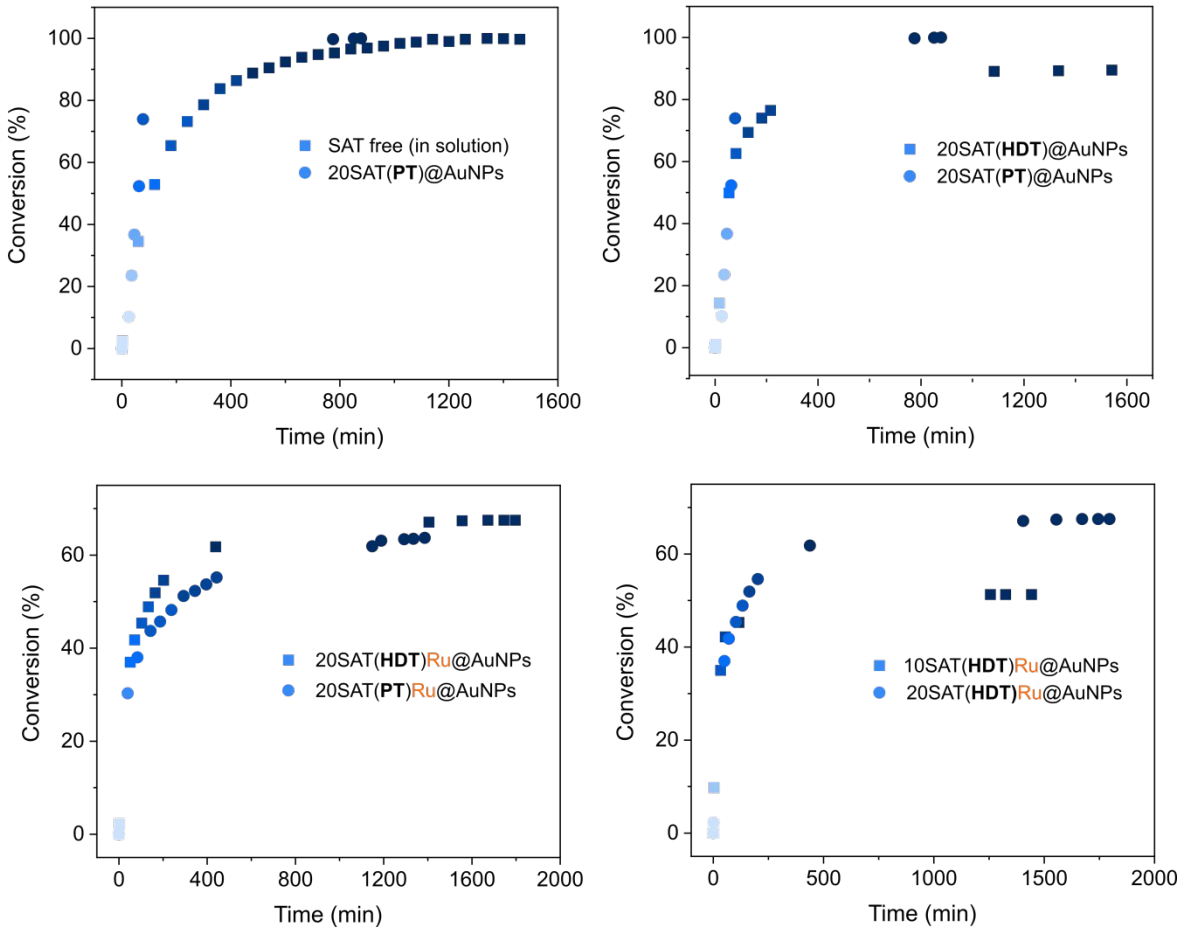

Figure S32. Comparative kinetics of the back isomerization of free SAT (0.006 mM) and SAT immobilized on AuNPs (0.14 mM in terms of Au) at different ratios in the presence of different background ligands with/without Ru. As can be seen, the presence of Ru has the most significant influence on the isomerization behaviour of SAT.

7. Catalytic experiments

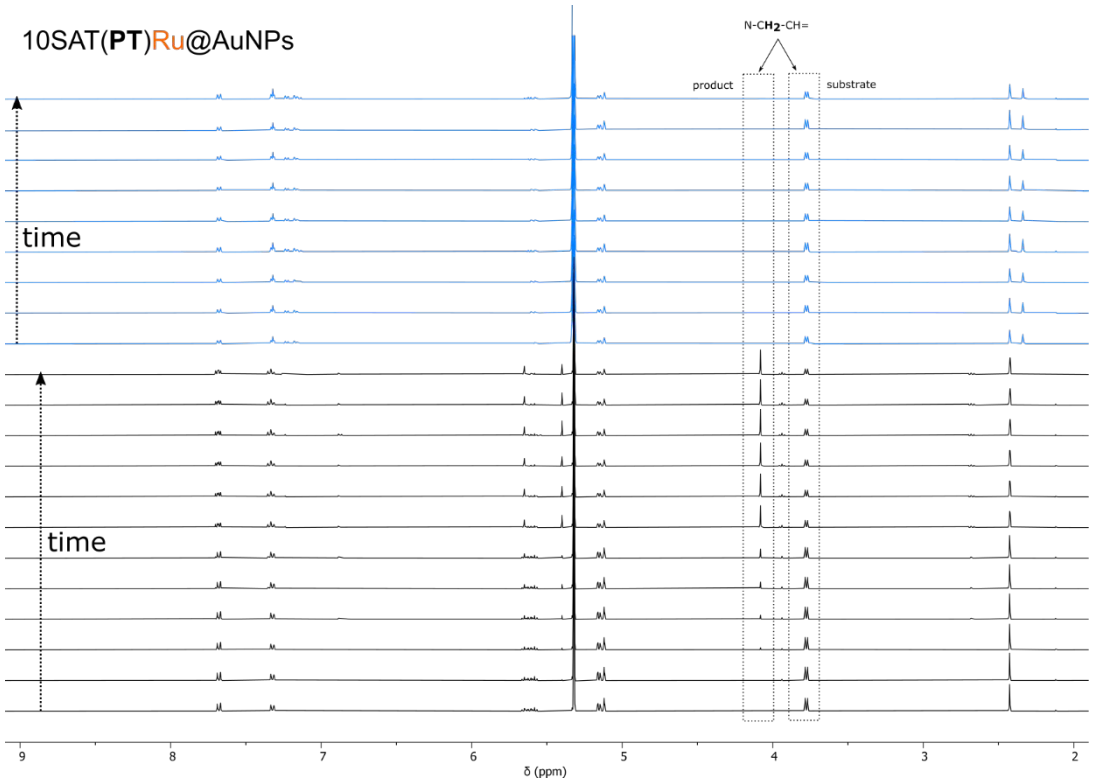

Figure S33. Time-resolved ^{1}H NMR spectra of the progress of metathesis reaction catalyzed by 10SAT(PT)Ru@AuNPs for nonirradiated (black) and preirradiated (blue) samples.

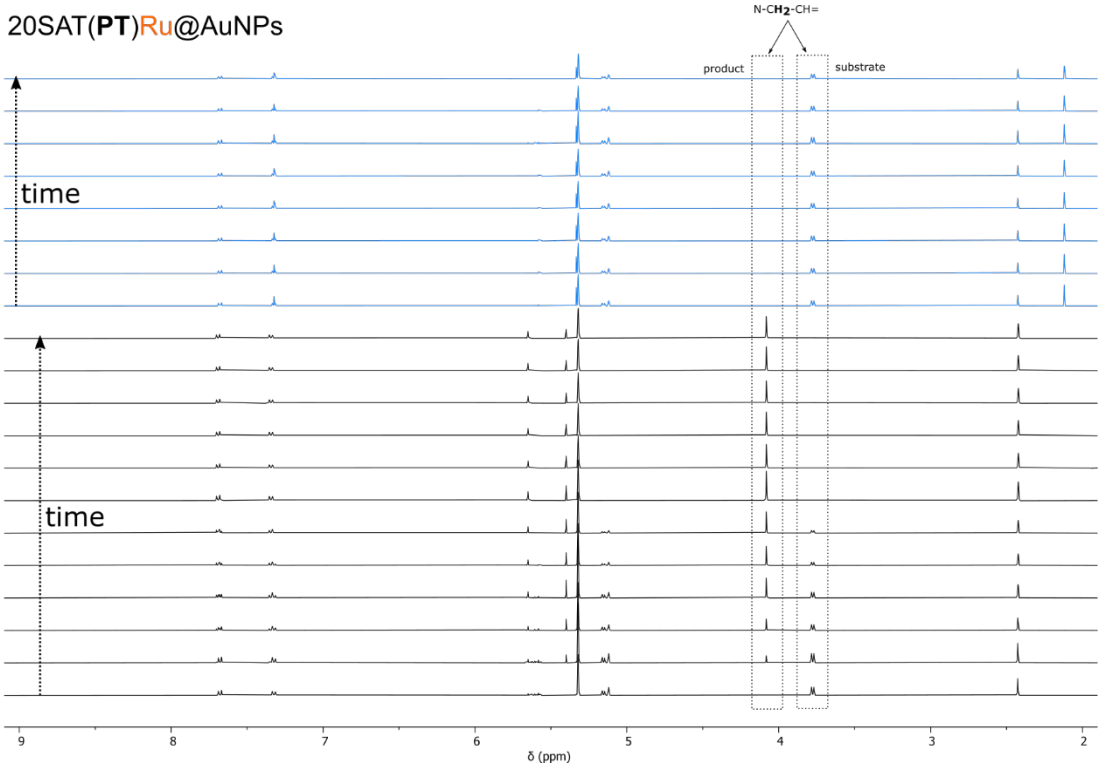

Figure S34. Time-resolved ^{1}H NMR spectra of the progress of metathesis reaction catalyzed by 20SAT(PT)Ru@AuNPs for nonirradiated (black) and preirradiated (blue) samples.

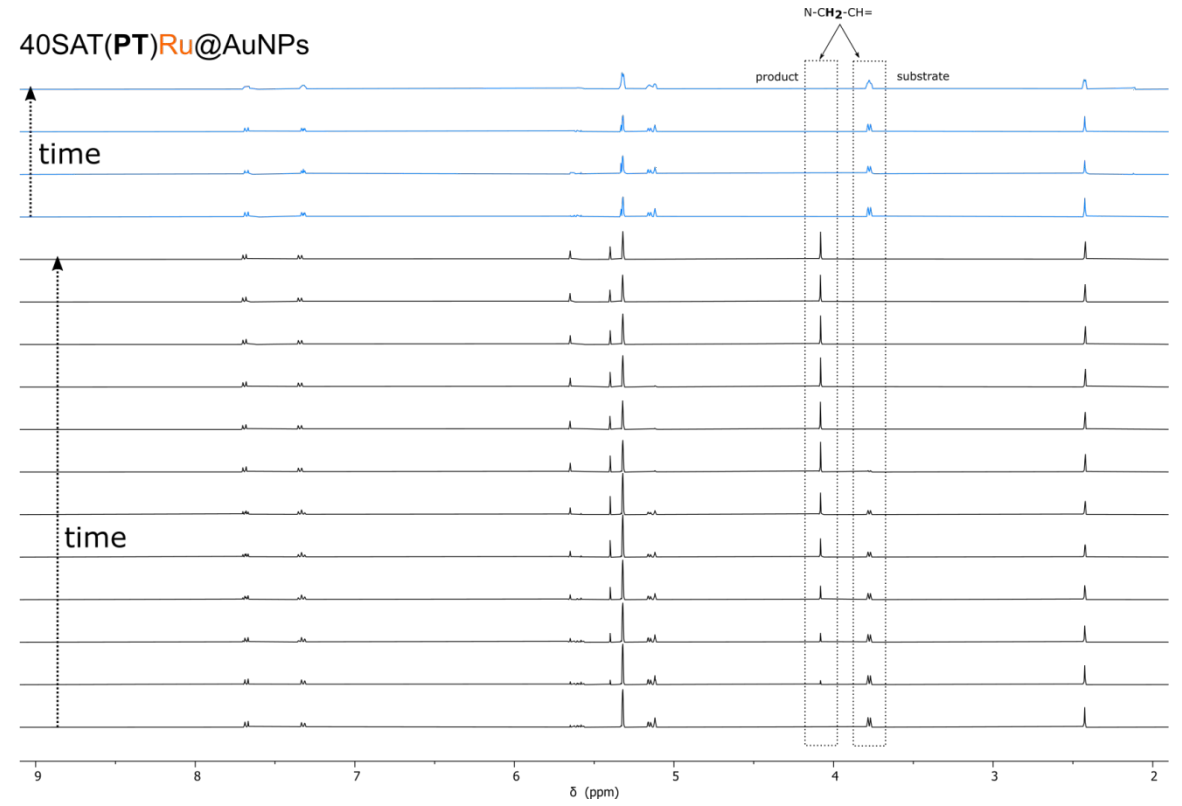

Figure S35. Time-resolved ^{1}H NMR spectra of the progress of metathesis reaction catalyzed by 40SAT(PT)Ru@AuNPs for nonirradiated (black) and preirradiated (blue) samples.

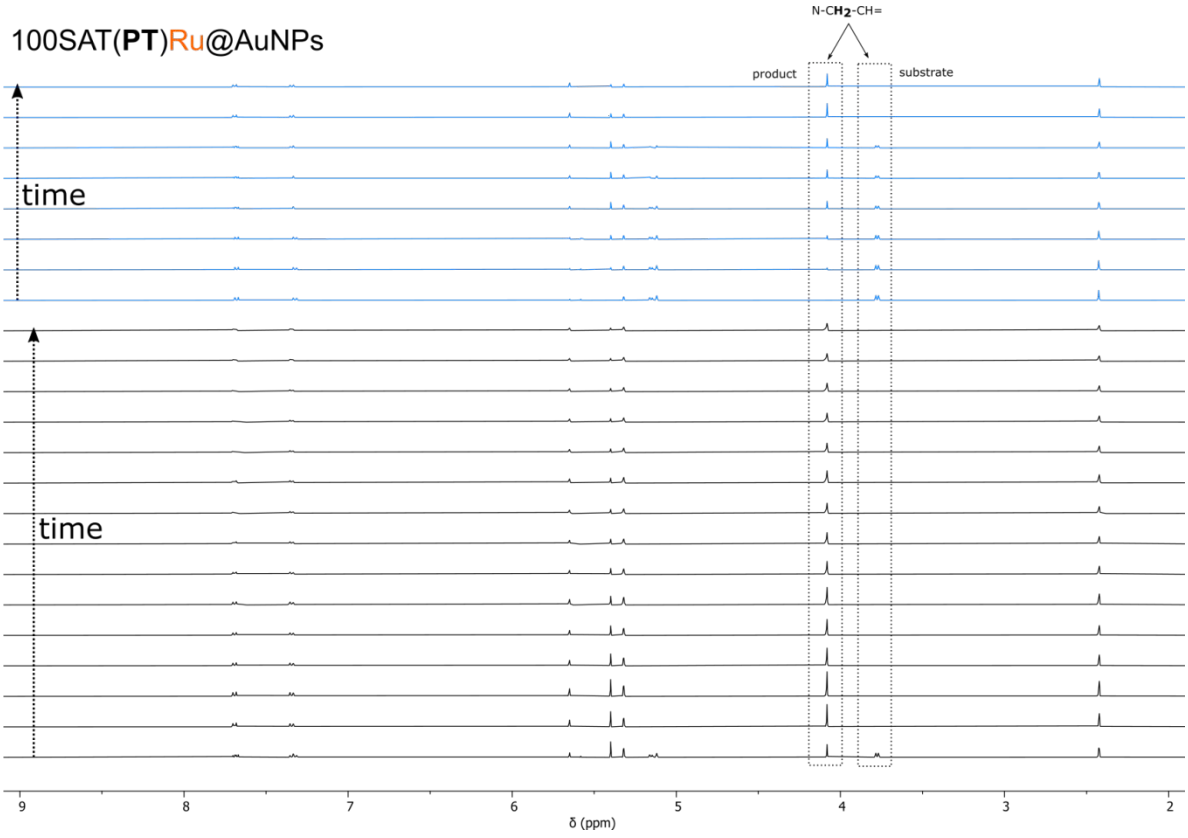

Figure S36. Time-resolved ^{1}H NMR spectra of the progress of metathesis reaction catalyzed by 100SAT(PT)Ru@AuNPs for nonirradiated (black) and preirradiated (blue) samples.

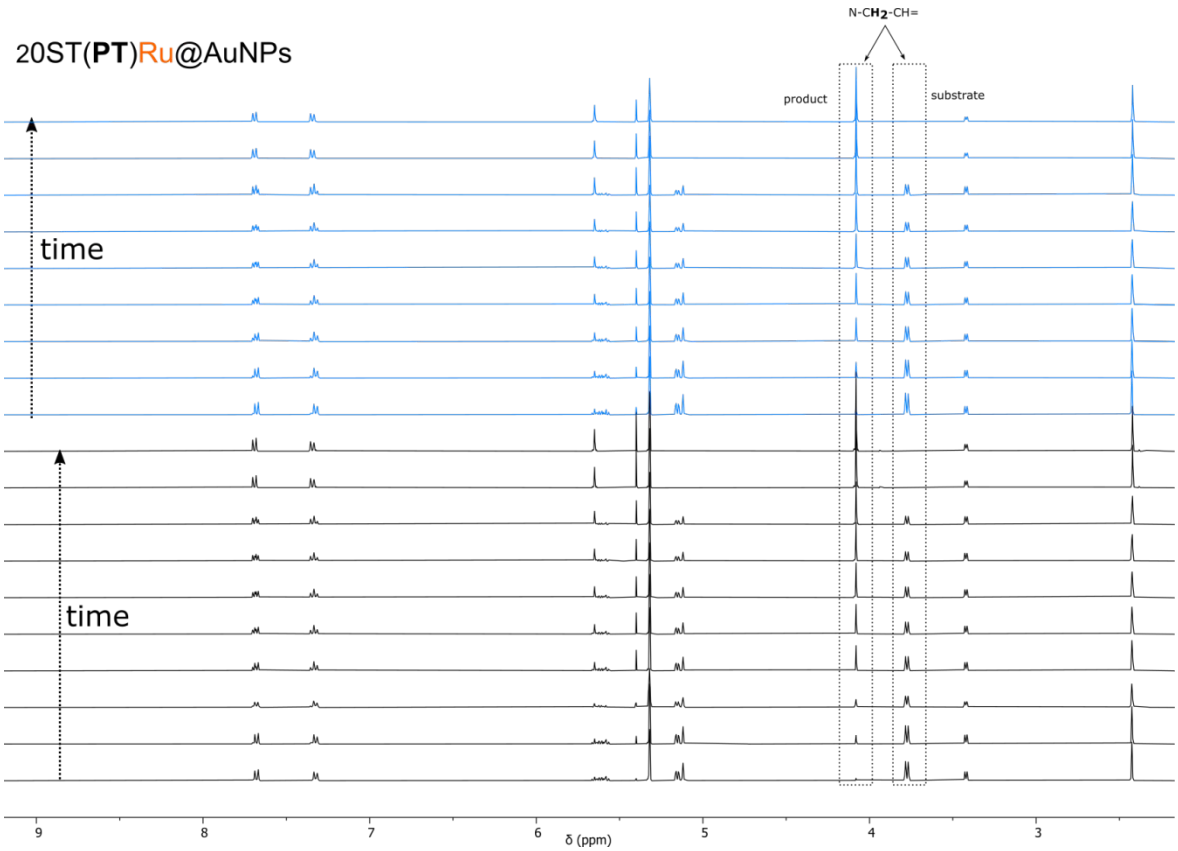

Figure S37. Time-resolved ^{1}H NMR spectra of the progress of metathesis reaction catalyzed by 20ST(PT)Ru@AuNPs for nonirradiated (black) and preirradiated (blue) samples.

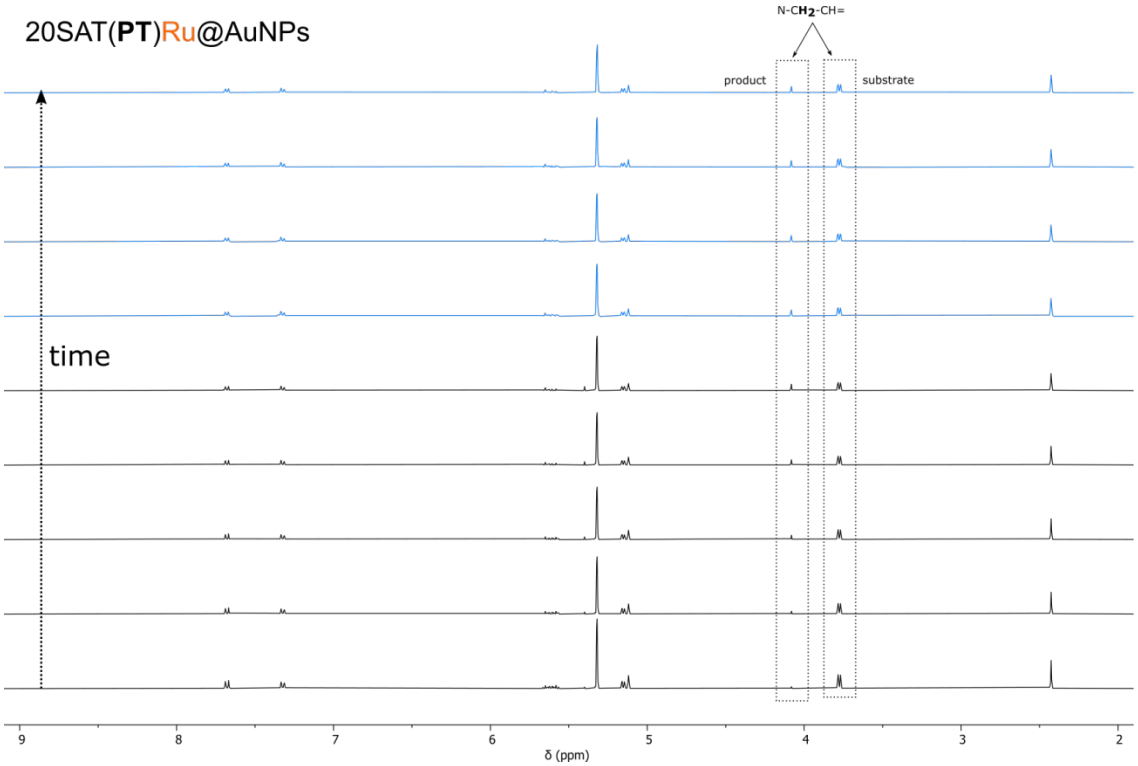

Figure S38. Time-resolved ^{1}H NMR spectra of the progress of metathesis reaction catalyzed by 20SAT(PT)Ru@AuNPs keeping the sample first in the dark (black), then in UV light (20 min), and again in the dark (blue).

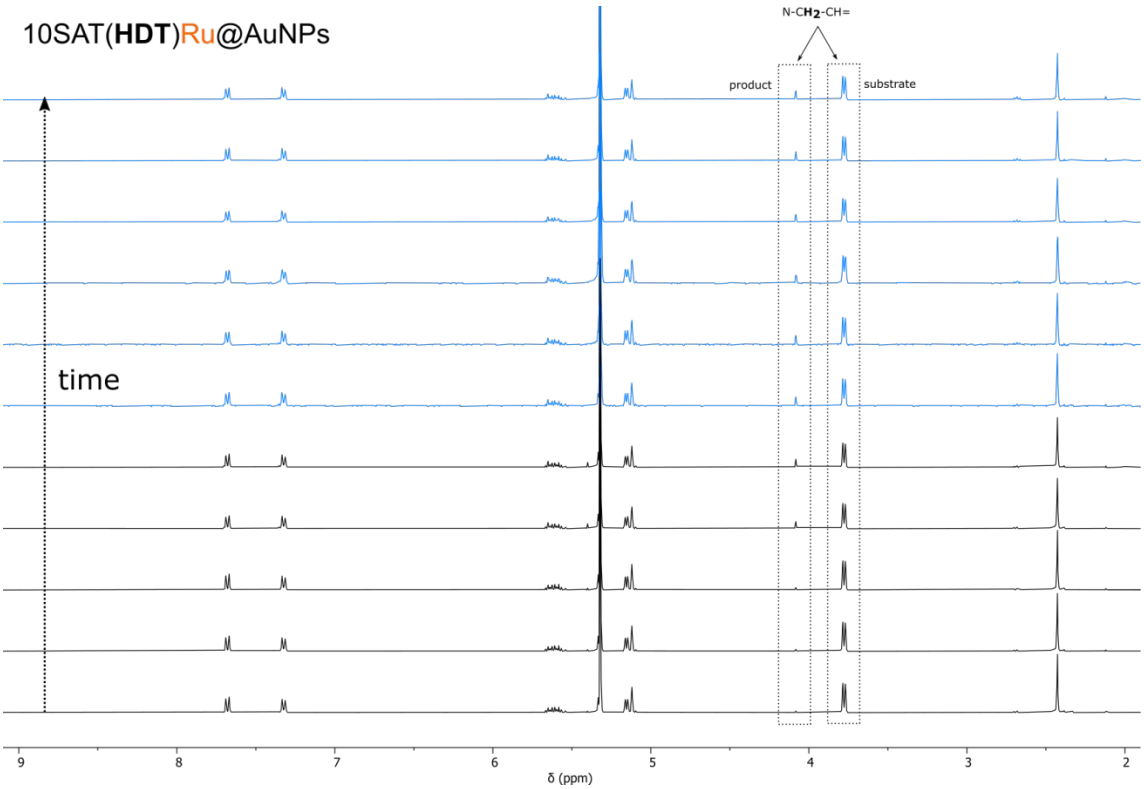

Figure S39. Time-resolved ^{1}H NMR spectra of the progress of metathesis reaction catalyzed by 10SAT(HDT)Ru@AuNPs keeping the sample first in the dark (black), then in UV light (20 min), and again in the dark (blue).

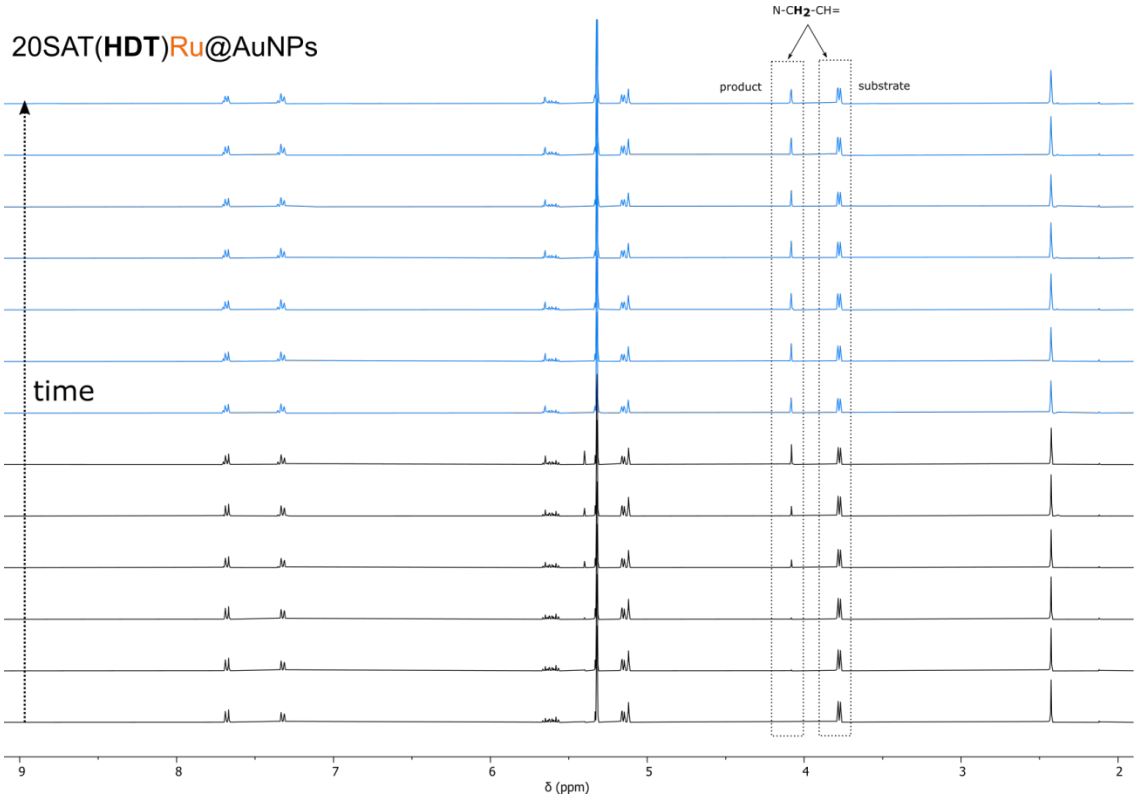

Figure S40. Time-resolved ^{1}H NMR spectra of the progress of metathesis reaction catalyzed by 20SAT(HDT)Ru@AuNPs keeping the sample first in the dark (black), then in UV light (20 min), and again in the dark (blue).

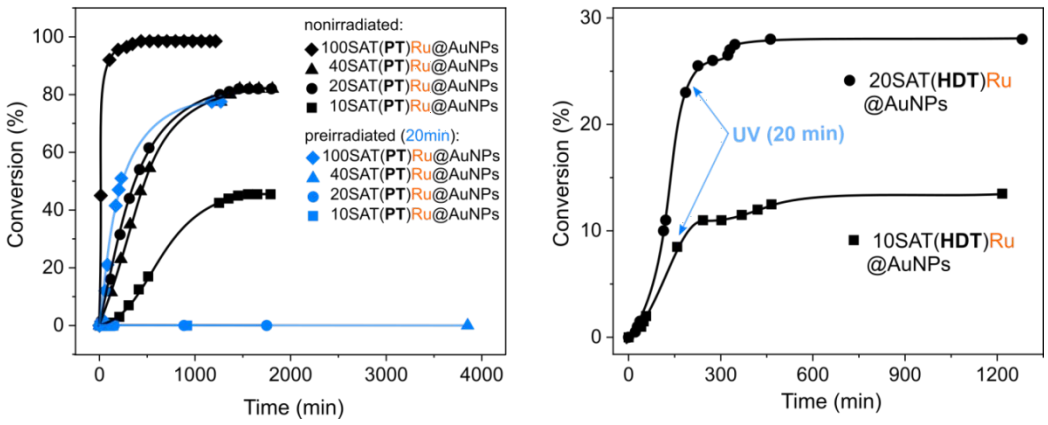

Figure S41. Comparative kinetics of metathesis reaction catalyzed by SAT/Ru coated AuNPs with PT and HDT ligands at different ratios and irradiation conditions. In all cases, the molar ratio between the immobilized SAT ligand and substrate was kept constant (1:10).

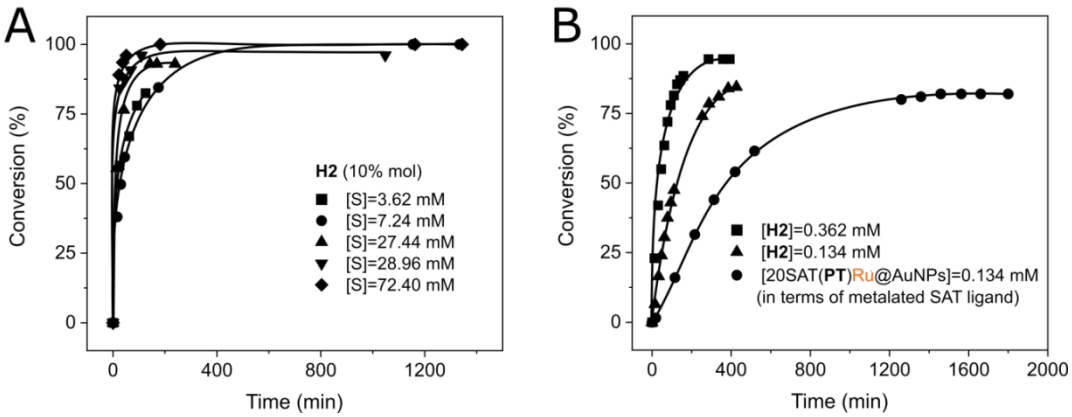

Figure S42. (A) Metathetical activity of free **H2** at different substrate concentrations while maintaining a constant precatalyst loading (10% mol); (B) Comparison of the metathetical activity of free (10 % mol and 3.7 % mol precatalyst loading) and immobilized **H2** (3.7 % mol precatalyst loading).

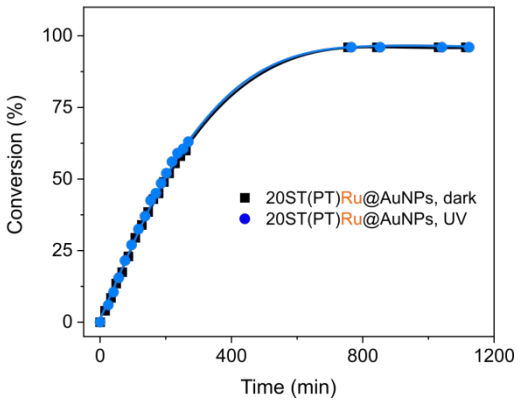

Figure S43. Comparative kinetics of metathesis reaction catalyzed by 20ST(PT)Ru@AuNPs (0.14 mM in terms of Au) in the dark and UV light. The molar ratio between the immobilized ST ligand and substrate was 1:10.

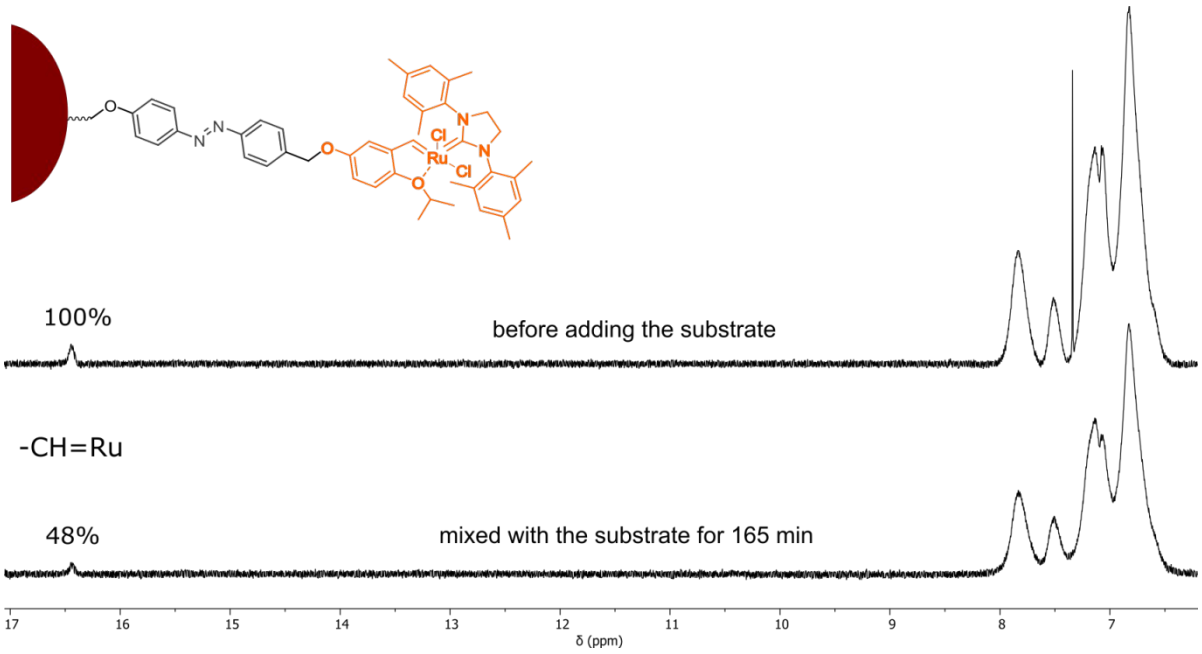

Figure S44. Partial ^{1}H NMR spectra of 20SAT(PT)Ru@AuNPs before and after mixing with the substrate for 165 min (before measurement, the NPs were purified by the redispersion-precipitation method), showing the partial initiation of the immobilized precatalyst, DCM-d_2, 298 K.

8. Additional computational results

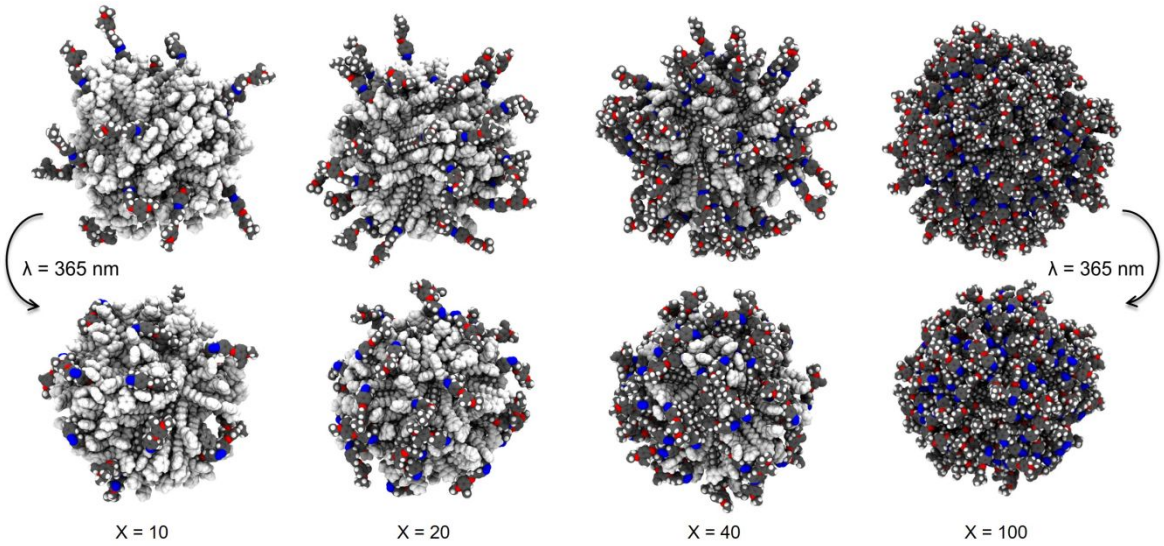

Figure S45. Molecular structure of χSAT(**PT**)@AuNPs extracted from equilibrated atomistic simulations as a function of the monolayer composition χ; χ =10, 20, 40, 100. SAT ligands are initially considered in the *trans* form (top row) and then converted in the *cis* form (bottom row). SAT chains are coloured by element (C, grey; N, blue; O, red, H, white) and PT chains as white spheres.

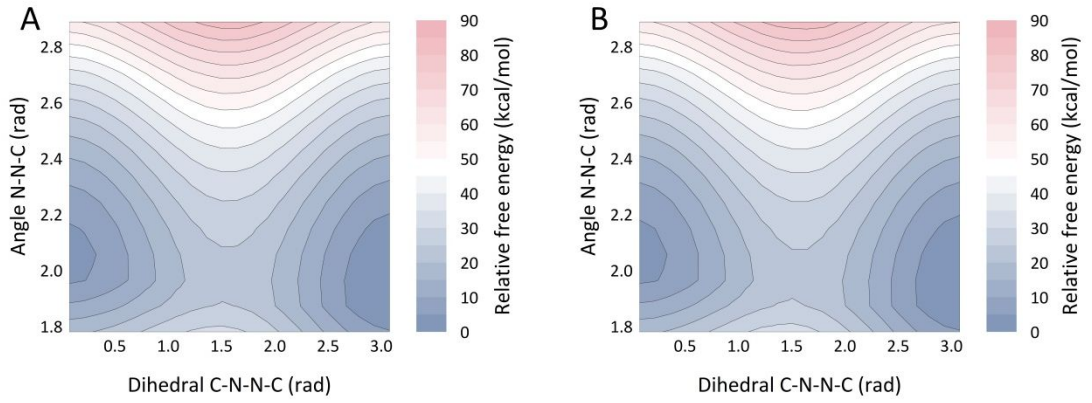

Figure S46. Free energy landscape for *cis* → *trans* isomerization as a function of the CNNC dihedral angle and the NNC angle for (a) the free SAT ligand and (b) one bound SAT ligand in 100SAT(**PT**)@AuNP with neighbouring SAT ligands in *trans* state. 2D maps are obtained from umbrella sampling calculations.

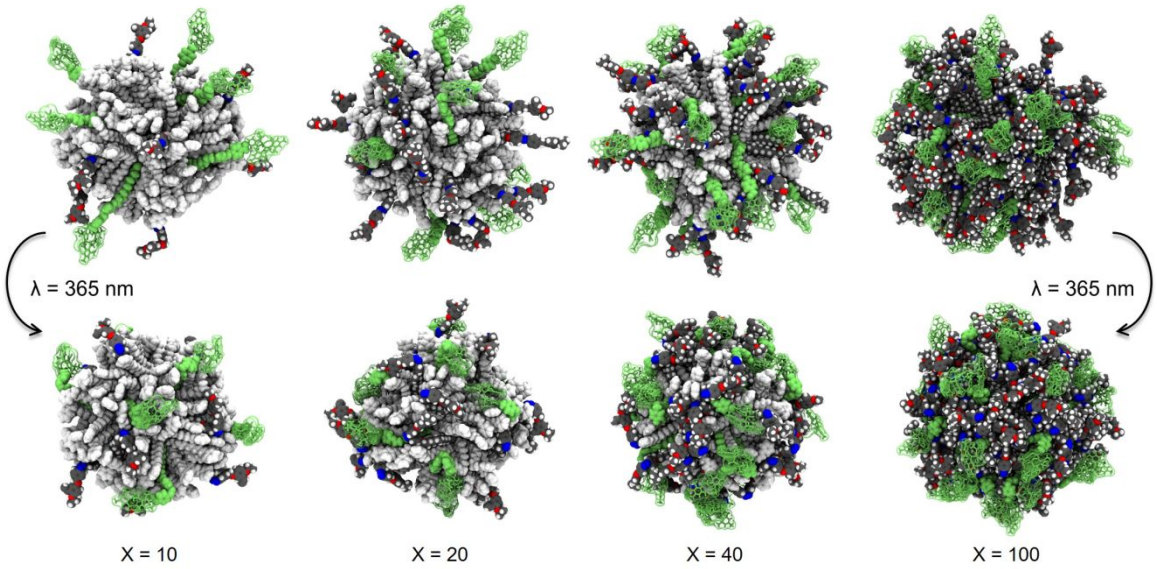

Figure S47. Molecular structure of χSAT(**PT**)Ru@AuNPs extracted from equilibrated atomistic simulations as a function of the monolayer composition χ; χ =10, 20, 40, 100. SAT ligands are initially considered in the *trans* form (top row) and then converted in the *cis* form (bottom row). SAT chains are colored by element (C, grey; N, blue; O, red, H, white), with those presenting the catalytic group in green, and PT chains are portrayed as white spheres. The Hoveyda-Grubbs moiety is highlighted as a green transparent surface.

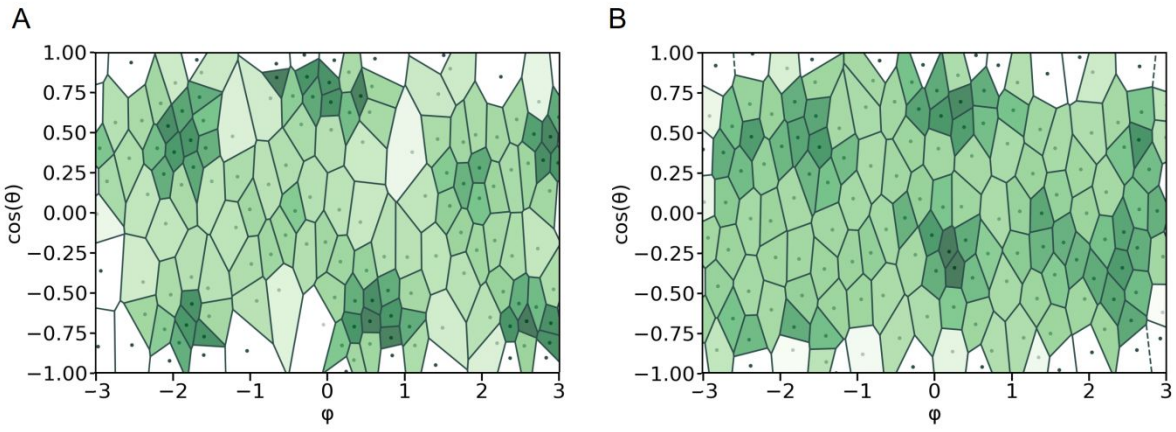

Figure S48. Voronoi tessellation based on the centre of mass (COM) of the ligands projected onto a bi-dimensional (φ, cos (θ)) plane for 20SAT(**HDT**)@AuNPs (A) and 20SAT(**PT**)@AuNPs (B). Each dot corresponds to a different COM. Each polygon is coloured according to its value, where darker (lighter) regions represent smaller (larger) area with higher (lower) ligand density with respect to the average.

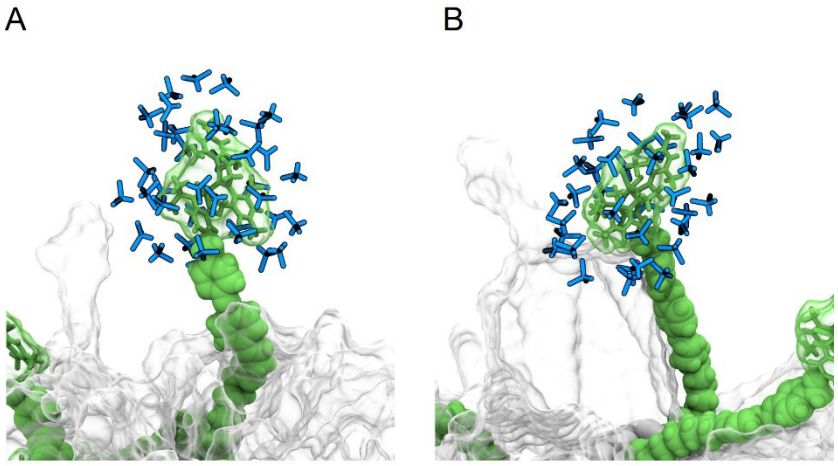

Figure S49. Visual comparison of solvent molecules in close contact (in blue) with the precatalytic group in 20SAT(PT)Ru@AuNPs (A) and 20SAT(HDT)Ru@AuNPs (B), showing one SAT(Ru) ligand (in green) as a representative example. SAT ligands are in *trans* conformation.

9. References

1. Larsen, A. H.; Mortensen, J. J.; Blomqvist, J.; Castelli, I. E.; Christensen, R.; Dułak, M.; Friis, J.; Groves, M. N.; Hammer, B.; Hargus, C.; Hermes, E. D.; Jennings, P. C.; Jensen, P. B.; Kermode, J.; Kitchin, J. R.; Kolsbjerg, E. L.; Kubal, J.; Kaasbjerg, K.; Lysgaard, S.; Maronsson, J. B.; Maxson, T.; Olsen, T.; Pastewka, L.; Peterson, A.; Rostgaard, C.; Schiøtz, J.; Schütt, O.; Strange, M.; Thygesen, K. S.; Vegge, T.; Vilhelmsen, L.; Walter, M.; Zeng, Z.; Jacobsen, K. W., The Atomic Simulation Environment—A Python library for working with atoms *J. Phys.: Condens. Matter* **2017**, 29,273002.
2. Heinz, H.; Lin, T.-J.; Kishore Mishra, R.; Emami, F. S. Thermodynamically consistent force fields for the assembly of inorganic, organic, and biological nanostructures: The INTERFACE force field *Langmuir* **2013**, *29*, 1754-1765.
3. He, X.; Man, V. H.; Yang, W.; Lee, T.-S.; Wang, J. A fast and high-quality charge model for the next generation general AMBER force field *J. Chem. Phys.* **2020**, *153*, 114502.
4. Vanquelef, E.; Simon, S.; Marquant, G.; Garcia, E.; Klimerak, G.; Delepine, J. C.; Cieplak, P.; Dupradeau, F.-Y., R.E.D. Server: a web service for deriving RESP and ESP charges and building force field libraries for new molecules and molecular fragments, *Nucl. Acids Res.* (Web server issue) **2011**, 39, W511-W517.
5. Wang, F.; Becker, J.-P.; Cieplak, P.; Dupradeau, F.-Y., R.E.D. Python: Object oriented programming for Amber force fields, Université de Picardie - Jules Verne, Sanford Burnham Prebys Medical Discovery Institute, Nov. **2013.**
6. Dupradeau, F.-Y.; Pigache, A.; Zaffran, T.; Savineau, C.; Lelong, R; Grivel, N.; Lelong, D.; Rosanski, W.; Cieplak, P., The R.E.D. tools: Advances in RESP and ESP charge derivation and force field library building, *Phys. Chem. Chem. Phys.* **2010**, 12, 7821-7839.
7. Bayly, C. I.; Cieplak, P.; Cornell, W.; Kollman, P. A., A well-behaved electrostatic potential based method using charge restraints for deriving atomic charges: the RESP model, *J. Phys. Chem.*, **1993**, 97, 10269-10280.
8. Gaussian 16, Revision C.01, Frisch, M. J.; Trucks, G. W.; Schlegel, H. B.; Scuseria, G. E.; Robb, M. A.; Cheeseman, J. R.; Scalmani, G.; Barone, V.; Petersson, G. A.; Nakatsuji, H.; Li, X.; Caricato, M.; Marenich, A. V.; Bloino, J.; Janesko, B. G.; Gomperts, R.; Mennucci, B.; Hratchian, H. P.; Ortiz, J. V.; Izmaylov, A. F.; Sonnenberg, J. L.; Williams-Young, D.; Ding, F.; Lipparini, F.; Egidi, F.; Goings, J.; Peng, B.; Petrone, A.; Henderson, T.; Ranasinghe, D.; Zakrzewski, V. G.; Gao, J.; Rega, N.; Zheng, G.; Liang, W.; Hada, M.; Ehara, M.; Toyota, K.; Fukuda, R.; Hasegawa, J.; Ishida, M.; Nakajima, T.; Honda, Y.; Kitao, O.; Nakai, H.; Vreven, T.; Throssell, K.; Montgomery, J. A., Jr.; Peralta, J. E.; Ogliaro, F.; Bearpark, M. J.; Heyd, J. J.; Brothers, E. N.; Kudin, K. N.; Staroverov, V. N.; Keith, T. A.; Kobayashi, R.; Normand, J.; Raghavachari, K.; Rendell, A. P.; Burant, J. C.; Iyengar, S. S.; Tomasi, J.; Cossi, M.; Millam, J. M.; Klene, M.; Adamo, C.; Cammi, R.; Ochterski, J. W.; Martin, R. L.; Morokuma, K.; Farkas, O.; Foresman, J. B.; Fox, D. J. Gaussian, Inc., Wallingford CT, 2016.
9. Heinz, H.; Vaia, R. A.; Koerner, H.; Farmer, B. L., Photoisomerization of azobenzene grafted to layered silicates: simulation and experimental challenges *Chem. Mater.* **2008**, *20*, 6444–6456.
10. Choi, J.; Chung, H.; Yun, J.-H.; Cho, M., Molecular dynamics study on the photothermal actuation of a glassy photoresponsive polymer reinforced with gold nanoparticles with size effect *ACS Appl. Mater. Interfaces* **2016**, *8* (36), 24008–24024.
11. Koch, M.; Saphiannikova, M.; Guskova O., Do columns of azobenzene stars disassemble under light illumination? *Langmuir* **2019**, *35* (45), 14659–14669.
12. Núñez-Zarur, F.; Solans-Monfort, X.; Roser Pleixats, R.; Rodríguez-Santiago, L.; Sodupe, M. DFT study on the recovery of Hoveyda–Grubbs-type catalyst precursors in enyne and diene ring-closing metathesis *Chem. Eur. J.* **2013**, *19*, 14553 – 14565.
13. Becke, A. D., Density-functional thermochemistry. III. The role of exact exchange *J. Chem. Phys.* **1993**, *98*, 5648–5652.
14. Hehre, W. J.; Ditchfield, R.; Pople, J. A., Self—consistent molecular orbital methods. XII. Further extensions of Gaussian—type basis sets for use in molecular orbital studies of organic molecules *J. Chem. Phys.***1972**, *56*, 2257–2261.

15. Francl, M. M.; Pietro, W. J.; Hehre, W. J.; Binkley, J. S.; Gordon, M. S.; Defrees, D. J.; Pople, J. A., Self-consistent molecular orbital methods. XXIII. A polarization-type basis set for second-row elements *J. Chem. Phys.***1982**, *77*, 3654–3665.
16. Küechle, W.; Dolg, M.; Stoll, H.; Preuss, H., *Mol. Phys. Ab initio* pseudopotentials for Hg through Rn **1991**, *74*, 1245–1263.
17. Bergner, A.; Dolg, M.; Kuchle, W.; Stoll, H.; Preuss, H., *Ab initio* energy-adjusted pseudopotentials for elements of groups 13–17 *Mol. Phys.* **1993**, *80*, 1431–1441.
18. Núñez-Zarur, F.; Poater, J.; Rodríguez-Santiago, L. R.; Solans-Monfort, X.; Solà, M.; Sodupe, M., On the electronic structure of second generation Hoveyda–Grubbs alkene metathesis precursors *Comput. Theor. Chem.* **2012**, *996*, 57-67.
19. Neese, F., The ORCA program system *Wiley Interdiscip. Rev.: Comput. Mol. Sci.* **2012**, *2*, 73-78.
20. Zheng, Q.; Tang, Q.; He, J.; Du, S.; Xu, S.; Wang, C.; Xu, Y.; Lin, F., VFFDT: A new software for preparing AMBER force field parameters for metal-containing molecular systems *J. Chem. Inf. Model.* **2016**, *56*, 811–818.
21. Case, D. A.; Ben-Shalom, I. Y.; Brozell, S. R.; Cerutti, D. S.; Cheatham, I. T. E.; Cruzeiro, L V. W. D.; Darden, T. A.; Duke, R. E.; Ghoreishi, D.; Gilson, M. K.; H. Gohlke, H.; Goetz, A. W.; Greene, D.; Harris, R.; Homeyer, N.; Izadi, S.; Kovalenko, A.; Kurtzman, T.; Lee, T. S.; LeGrand, S.; Li, P.; Lin, C.; Liu, J.; Luchko, T.; Luo, R.; Mermelstein, D. J.; Merz, K. M.; Miao, Y.; Monard, G.; Nguyen, C.; Nguyen, H.; Omelyan, I.; Onufriev, A.; Pan, F.; Qi, R.; Roe, D. R.; Roitberg, A.; Sagui, C.; Schott-Verdugo, S.; Shen, J.; Simmerling, C. L.; Smith, J.; Salomon-Ferrer, R.; Swails, J.; Walker, R. C.; Wang, J.; Wei, H.; Wolf, R. M.; Wu, X.; Xiao, L.; York D. M.; Kollman, P. A., AMBER **2018**, University of California, San Francisco.
22. Salomon-Ferrer, R.; Goetz, A. W.; Poole, D.; Le Grand, S.; Walker, R. C., Routine microsecond molecular dynamics simulations with AMBER - Part II: Particle Mesh Ewald *J. Chem. Theory Comput.* **2013**, *9*, 3878-3888.

23. Goetz, A. W.; Williamson, M. J.; Xu, D.; Poole, D.; Le Grand, S.; Walker, R. C., Routine microsecond molecular dynamics simulations with AMBER - Part I: Generalized Born *J. Chem. Theory Comput*. **2012**, *8*, 1542-1555.
24. Le Grand, S.; Goetz, A. W.; Walker, R. C., SPFP: Speed without compromise - a mixed precision model for GPU accelerated molecular dynamics simulations *Comp. Phys. Comm*. **2013**, *184*, 374-380.
25. Grossfield, A., "WHAM: an implementation of the weighted histogram analysis method", http://membrane.urmc.rochester.edu/content/wham/, version 2.0.11.
26. Ferrenberg, A. M.; Swendsen, R. H., Optimized Monte Carlo data analysis *Phys. Rev. Lett.***1989**, *63*, 1195–1198.
27. Kumar, S.; Bouzida, D.; Swendsen, R. H.; Kollman, P. A.; Rosenberg, J. P., THE weighted histogram analysis method for free-energy calculations on biomolecules. I. The method *J. Comput. Chem.* **1992**, *13*, 1011-1021.
28. Kumar, S.; Rosenberg, J. M.; Bouzida, D.; Swendsen, R. H.; Kollman P. A. Multidimensional free-energy calculations using the weighted histogram analysis method *J. Comput. Chem.* **1995**, *16*, 1399-1350.
29. Sashuk, V., Thiolate-Protected Nanoparticles via Organic Xanthates: Mechanism and Implications *ACS Nano* **2012**, *6,* 10855-10861.
30. Wang, Y.; Yu, J.; Wang, Z.; Iqbal, S.; Zhang, W.; Zhang, Z.; Zhou, N.; Zhu, X., Real-time near-infrared fluorescence reporting the azoreductase-triggered drug release. *Polym. Chem.* **2020,** *11*, 734-743.
31. Chen, S.-W.; Kim, J. H.; Song, C. E.; Lee, S.-g., Self-Supported Oligomeric Grubbs/Hoveyda-Type Ru−Carbene Complexes for Ring-Closing Metathesis. *Org. Lett.* **2007,** *9*, 3845-3848.
32. Sobczak, G.; Misztalewska-Turkowicz, I.; Sashuk, V., Photoswitching, Colloidal Stability, and Reversible Self-Assembly of Gold Nanoparticles Covered with Thiolated Donor–Acceptor Stenhouse Adducts. *J. Phys. Chem. C* **2021,** *125*, 5306-5314.
33. Fischer, S.; Ward, T. R.; Liang, A. D., Engineering a Metathesis-Catalyzing Artificial Metalloenzyme Based on HaloTag. *ACS Catal.* **2021,** *11*, 6343-6347.